Visible-light photocatalysts: Prospects and challenges

Cite as: APL Mater. 8, 030903 (2020); doi: 10.1063/1.5140497
Submitted: 28 November 2019 • Accepted: 20 February 2020 •
Published Online: 10 March 2020

Aleksandra B. Djurišić,[1,a)] Yanling He,[1,2] and Alan M. C. Ng[2]

AFFILIATIONS

[1] Department of Physics, The University of Hong Kong, Pokfulam Road, Hong Kong
[2] Department of Physics, South University of Science and Technology, 518055 Shenzhen, China

[a)] Author to whom correspondence should be addressed: dalek@hku.hk

ABSTRACT

In this research update, we discuss the visible-light photocatalysis. Due to the potential of utilizing freely available solar energy for environmental remediation and fuel generation, this topic has been of increasing interest. Huge amount of work has been done in developing a large variety of photocatalyst materials, and advances have been made in understanding the process. Nevertheless, substantial challenges remain. Some of those challenges could possibly be solved by developing better materials, but in many cases, the biggest problem is whether photocatalysis could be scaled up to an industrial process that would be cost-competitive to existing technologies. Here, we discuss different types of visible-light photocatalysts and their applications and outline various challenges that need to be addressed in the development of practically relevant materials and systems.

I. INTRODUCTION

Due to its potential for green energy and environmental remediation, photocatalysis has been attracting increasing attention in recent years. Consequently, there are many reviews on this topic, focusing on different types of photocatalysts and different photocatalyst applications.[1–9] Considering the abundance of existing review papers on photocatalysis (over 2700 reviews since 2015, out of which over 1500 discuss visible or solar photocatalysis), in this article, we aim to provide a novel perspective on the issue by concise description of the problems and key strategies to tackle these problems, with selected examples of those strategies. Due to a huge number of published papers, providing a comprehensive overview of everything that has been reported even within a short time frame would be a daunting and not a particularly useful task since the abundance of data would cloud the key issues that need to be addressed. Furthermore, in the last five years, there have been limited fundamental advances in concepts and no significant breakthroughs in photocatalyst design. The principles are known, incremental progress has been made, and there is still lots of work to be done both in making these materials practically relevant (which is questionable for some applications) and in improving our understanding of the complex processes, in particular, in some complicated ternary or quaternary photocatalysts proposed.

The interest in photocatalysis has been rising since seminal works by Honda and Fujishima in 1972[10] and Reiche and Bard in 1979.[11] Various photocatalyst materials and photocatalytic applications have been investigated since then, but the commercial applications of photocatalysis have been scarce. The scarcity of commercial applications is typically attributed to the low photocatalytic activity, in particular, under visible or solar illumination.[1] Consequently, considerable efforts have been devoted into the development of photocatalyst materials with improved performance. Similarly, significant efforts have been devoted to the design of photocatalytic reactors, but this topic is beyond the scope of this review. When it comes to material design and different types of photocatalysts, the material development strategies are focused on maximizing the efficiency by targeting one or more steps in the photocatalytic reaction. The first step is the light absorption and the formation of the photogenerated electron–hole pairs.[1] The photogenerated carriers, then, migrate, and they can either recombine or reach the surface where they can participate in surface redox reactions.[1] Therefore, the strategies aiming at the improvement of photocatalytic performance target maximizing the absorption of light, maximizing charge

transfer at the surface, and minimizing recombination by achieving efficient charge separation and maximizing surface redox reactions.[1] To achieve these goals, preferably more than one at a time, common methods investigated for performance improvement are morphology optimization (which can affect the surface active sites, as well as charge separation), doping (which can reduce the bandgap but sometimes can have negative effects on recombination losses), using sensitizers and/or co-catalysts (to increase visible absorption as well as provide more active sites and affect carrier dynamics), and using different types of heterojunctions.[1] We will discuss different types of photocatalysts in Sec. II.

Then, we will discuss the challenges of different types of applications, and we will mainly focus on common environmentally relevant applications, namely, pollutant degradation and solar fuel applications. Other applications of photocatalysis, such as applications in synthetic chemistry, will be only briefly discussed. Before we proceed with that, it is worthwhile to examine some basic premises. The first question is whether photocatalysis is commercially viable. The idea itself is immensely attractive—the use of the low cost environmentally friendly materials and solar energy which is essentially free for water treatment or the generation of hydrogen or hydrocarbon fuels. The answer to this question depends on whether there are less expensive alternatives which are good enough to do the job. The second question is whether it is truly necessary to have efficient visible photocatalysis since there are inexpensive and efficient UV light sources. The answer to this question will depend on the actual numbers, i.e., efficiencies under different excitations, reactor designs, and energy costs and efficiencies [for example, parity violating (PV) system for powering up UV illumination]. The third and final question is whether the photocatalysts are truly environmentally friendly. The answer to this question would be that it depends on the synthesis method, the reactor design, and the possibility of uncontrolled discharge of photocatalysts into the environment. We will discuss these questions in detail in Sec. III on the applications of photocatalysts. Finally, we will provide a brief description of recent advances in characterization techniques, which can provide answers to fundamental questions concerning photocatalysts and photocatalytic reactions, and discuss future outlook of visible photocatalysts.

II. TYPES OF PHOTOCATALYSTS

Popular photocatalyst materials, either as single material photocatalysts or as parts of heterojunctions (including Z-scheme systems), as illustrated in Fig. 1, are TiO_2,[12–16] ZnO,[3,12,14] carbon nitride g-C_3N_4,[2,4,17] metal-organic framework (MOF) compounds,[8] graphene-based photocatalysts,[7] BiOCl,[18,19] black phosphorus,[20,21] $ZnFe_2O_4$,[22] etc. Among these materials, TiO_2 is still the one most commonly evaluated in different reactor designs, while g-C_3N_4 is an increasingly popular component of photocatalysts for fuel generation due to its lower bandgap (~2.8 eV), favorable conduction band (CB) edge position, and the abundance of surface groups that enable coupling to other photocatalysts.[23,24] However, graphitic carbon nitride has inferior chemical stability compared to TiO_2,[15] and it can be susceptible to degradation by hydroxyl radicals.[25] It can also exhibit high recombination rates, low conductivity, insufficient visible-light absorption, and low solvent-accessible surface area.[24] Consequently, great efforts have been made in modifying the structure of polymeric carbon nitride to improve its performance. Some recently proposed materials, for example, metal halide perovskites such as $CsPbBr_3$,[26] are also of interest, in particular, from the point of view of understanding the fundamental mechanisms in these remarkable materials. However, while there are many studies on designing novel photocatalysts, it should be noted that many materials investigated in research papers are unlikely to have practical application despite being promising in bench-scale evaluations.[15] Any material that contains toxic elements (CdS and $CsPbBr_3$, for example), or rare and expensive components, or is fragile or chemically unstable is unlikely to be practically relevant, which likely contributes to the popularity of TiO_2 photocatalysis.[15]

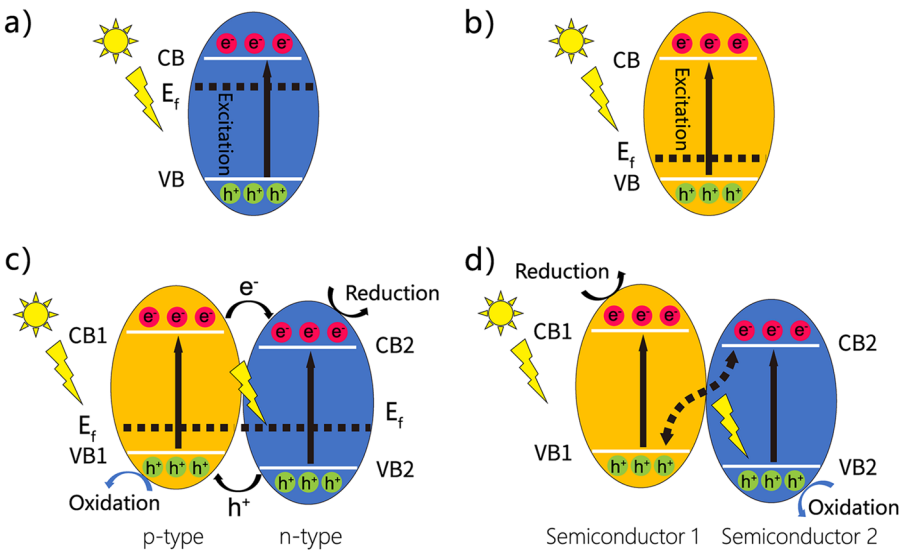

FIG. 1. Schematic diagram of different types of photocatalysts: [(a) and (b)] single material photocatalyst, (c) heterojunction photocatalyst, and (d) Z-scheme photocatalyst.

A. Single material photocatalysts

Single material photocatalysts (*n*-type and *p*-type semiconductors) are shown in Fig. 1. In addition to conventional semiconductor photocatalyst materials, MOFs have been attracting increasing attention recently. For a detailed review of MOFs for various photocatalytic applications, including hydrogen generation and CO_2 reduction, see Ref. 8. Similar to other photocatalysts, these materials still need significant improvements in achieved efficiencies, but they have been studied for considerably shorter time compared to conventional inorganic semiconductors.[8] In addition, organic polymers have also been attracting interest for photocatalysis applications.[27] Still, the majority of literature reports concern inorganic semiconductors, and hence, we will discuss those in more detail. However, the investigations of single material photocatalysts have been declining in popularity in recent years, mainly due to difficulties in simultaneously achieving narrow bandgap, favorable energy band alignments, and low recombination losses in a single material. Nevertheless, it is still worth mentioning common strategies for improving the performance of single material photocatalysts for visible-light photocatalysis since these strategies can still be employed to improve the performance of individual components of more complex photocatalysts. These strategies typically involve the optimization of crystal structure, surface area, and morphology; the manipulation of native defects; or the introduction of dopants to adjust the optical and electronic properties. In addition, sensitizers can be used to enhance the light absorption in the visible spectral range.

1. Surface engineering

The crystal structure of a semiconductor is known to affect its photocatalytic efficiency.[28] Since photocatalytic reactions occur at the active sites on the photocatalyst surface, the photocatalytic efficiency can be increased by nanostructure size and morphology optimization.[16] The number of active sites increases with the increase in the surface area, as well as the increase in the proportion of crystal facets with higher photocatalytic activity.[16,29] In general, morphological effects (for example, nanocrystals vs nanowires of the same material) on the photocatalytic activity can be interpreted as crystal facet-dependent reactivity or structural sensitivity.[28] Higher surface energy facets are thermodynamically unfavorable but can be achieved via careful optimization of the synthesis conditions.[16,29] In TiO_2, increased photocatalytic activity can be achieved by optimizing {101} (reducing sites) and {001} (oxidizing sites) facets, while in ZnO increased activity is achieved on zinc terminated polar {0001} facets.[29]

2. Defect engineering

Both cation[30–33] and anion[31,34] defects can affect photocatalytic activity. An example of the strategy of the use of native defects is using anion vacancies (oxygen vacancies[19] or nitrogen deficiency[35]) to control photocatalytic activity. In addition, it was shown that individual defects could have either positive or negative effects on the photocatalytic activity,[36] for example, the introduction of oxygen and nitrogen defects in g-C_3N_4 produced defects that are beneficial (O=C, $-NH_x$ species and N defects at the N-2C site) or detrimental (hydroxyl groups) for hydrogen evolution.[36] In addition to these possible defects, cyano group (C≡N) is another relevant defect in g-C_3N_4.[37] Native defects, such as oxygen vacancy, could not only introduce gap states to extend the photocatalytic response to longer wavelengths (depending on the semiconductor), but they can also enhance exciton dissociation, which contributes to enhanced charge carrier transfer and, consequently, photocatalytic activity.[34] Furthermore, defects can also serve as active sites for molecule chemisorption and alter the reaction pathways.[38] In addition to point defects (anion vacancies, cation vacancies, multivacancies, and interstitials), larger structural defects (edges in 2D materials and disorder) can contribute to photocatalytic activity. For example, surface disorder and native defects induced by reducing reactions in metal oxides (heating with a reducing agent) can result in a significant enhancement of visible-light absorption.[39] Furthermore, photocatalytic activity can also be affected by morphology optimization.[40–42] For example, in porous g-C_3N_4, enhanced hydrogen evolution and pollutant degradation were observed not only due to surface area increase but also due to improved charge carrier separation.[40] Increased photocatalytic activity for hydrogen generation was also reported for multishell g-C_3N_4.[41] For a detailed review of defect engineering in photocatalysis (for water splitting applications), see Ref. 43.

3. Doping

Doping is another relatively common method to extend the absorption response to longer wavelengths. It can also be used to modulate the growth of the photocatalyst to stabilize more reactive facets to enhance photocatalytic activity.[44] Common dopants for wide bandgap oxide photocatalysts, such as TiO_2 and ZnO, are nitrogen, sulfur, carbon, phosphorus, and fluorine as non-metal dopants and Ag, Mg, Cu, Rb, Co, Mo, Au, Pt, Fe, Cr, V, etc., as metal dopants.[12,15,45] Hydrogenation can also be used to extend the optical response of titania into the visible spectral range (i.e., black titania).[46,47] Nitrogen doping has been reported in porous carbon,[48] while dopants in g-C_3N_4 include oxygen, sulfur, nitrogen, iodine, bromide, and phosphorus.[37,49,50] In addition, alkali metal (Li^+, Na^+, and K^+)[51] and chlorine[52] doping has also been reported for g-C_3N_4. In addition to single dopants, co-doping can be used. Alternatively, doping and defect engineering can be combined for synergistic improvements in performance.[48] It should be noted that while doping can indeed extend the absorption into the visible range by introducing midgap states, those states can also act as recombination centers and increase recombination losses, while the shift in the redox potential can negatively affect the surface redox reactions.[15] Another approach to extend the absorption range into the visible is the formation of solid solutions, such as oxynitrides, GaN:ZnO, or InN:ZnO.[53,54]

4. Sensitizing

Increased visible-light absorption can be achieved using sensitizers. Sensitizers such as adsorbed organic dyes or metal complexes can be used for this purpose.[29] As an example, organic metal complexes, such as $Ru(bpy)_3^{2+}$ (bpy = 2′,2 bipyridine),[55] can be used as photosensitizers. It should be noted, however, that since sensitizing involves adsorption of the molecule on the surface, it can be dependent on the pH of the solution.[29] In addition, the presence of an electron donor is required to avoid the degradation of the sensitizer. Consequently, the popularity of organic sensitizers has been

in decline in recent years, and the majority of research efforts have focused on the various composite materials.

B. Semiconductor heterojunction photocatalysts

To extend the light absorption into the visible range, but without the drawback of increased recombination, metal–semiconductor or semiconductor–semiconductor heterojunctions can be used.[1,15] For a comprehensive review of heterojunction photocatalysts, see Ref. 1. In the following, we will discuss different types of heterojunction photocatalysts.

1. Common heterojunction photocatalysts

Heterojunction photocatalysts can be classified on the basis of energy band alignments (type I, type II, and type III), as illustrated in Fig. 2, or they can be classified based on material morphology, such as partial contact photocatalysts and core-shell photocatalysts. An important factor to consider in the heterojunction design for efficient photocatalytic activity is the band edge alignment.[56] The band edge alignment at the interface is affected by band bending when two materials come in contact, and it can be significantly affected by interface properties (surface dipoles, the presence of interfacial defects that result in trapped charges, etc.). In general, this is a common phenomenon affecting all heterojunctions and it has been extensively studied in various electronic and optoelectronic semiconductor devices. When it comes to photocatalysts, however, there are some distinctive features less commonly observed in layered structures in electronic devices. For example, the band alignment and band bending can be strongly dependent on the particle sizes and their arrangement on each other.[57] Facet dependence has also been observed in band bending, which affects the charge transport across interfaces of different contacting planes and, consequently, photocatalytic activity.[58] Furthermore, band bending not only occurs in junctions between different materials, or different crystal phases of the same material (heterophase junctions), but can also occur between large and small particles of the same material with the same crystal structure.[59] In this case, the difference in the surface band bending results in an electric field that drives the charge carrier separation.[59]

Depending on the morphology of two semiconductors, partial contact photocatalysts can have point contact where one of the photocatalysts is a nanoparticle, line contact for nanowire

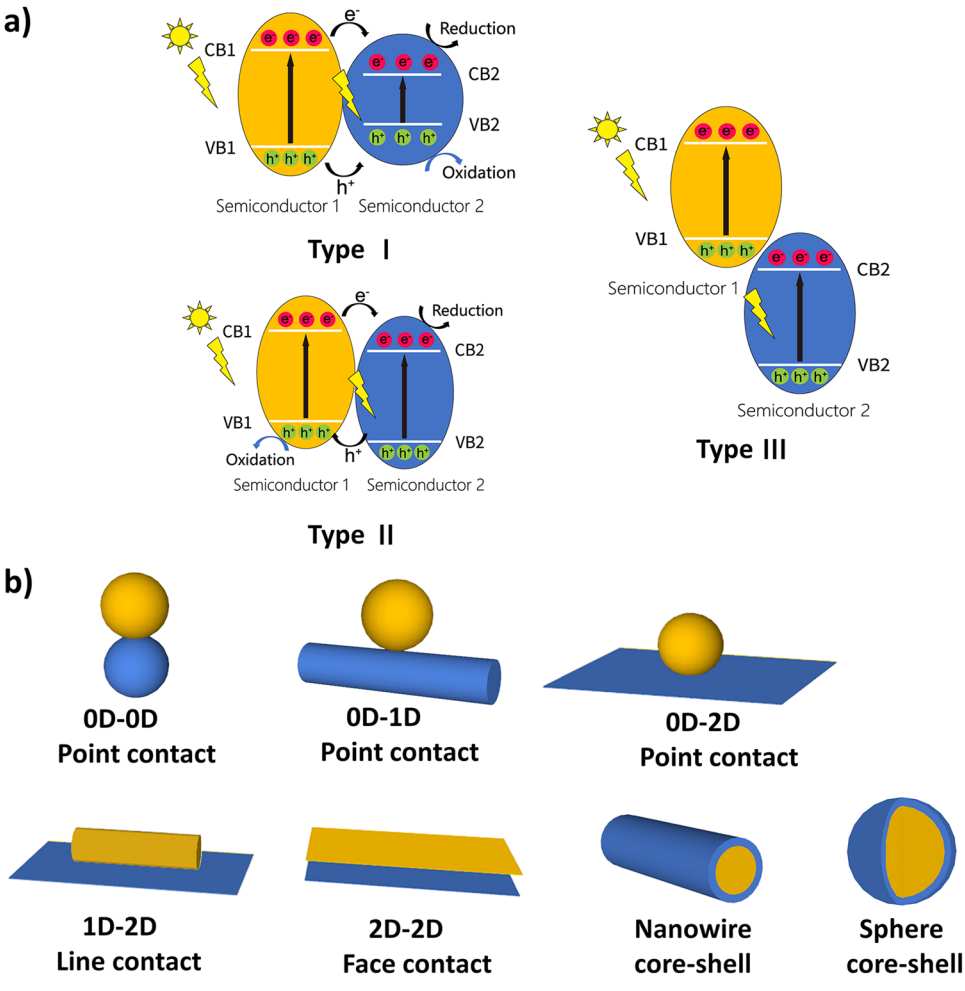

FIG. 2. (a) Schematic diagram of type I, II, and III heterojunction photocatalysts. (b) Schematic diagram of partial contact and core-shell photocatalysts.

or nanoribbon/nanosheet catalysts, and face contact when both photocatalysts are two dimensional.[1] In addition to energy levels and morphology, another consideration for the choice of materials to form a heterojunction is the lattice mismatch, with materials having low lattice mismatch being preferred.[60] Higher lattice mismatch will result in increased strain, which in turn can lead to the increased concentration of interfacial defects that can increase recombination losses and affect energy level alignment at the interface. Various heterojunction photocatalysts have been reported, such as CeO_2—AgI,[61] g-C_3N_4/Bi_2WO_6,[62] Ag_2O/Bi_5O_7I,[63] In_2S_3/$CdIn_2S_4$ nanotubes,[64] CdS/MoS_2,[65] amorphous NiO/g-C_3N_4,[66] ZnS/g-C_3N_4,[67] g-C_3N_4/$ZnIn_2S_4$,[68] g-C_3N_4/phosphorene,[69] $ZnIn_2S_4$—In_2O_3,[70] and p-$CaFe_2O_4$/n-$ZnFe_2O_4$.[56] In addition to more conventional heterojunctions involving common inorganic semiconductors, the combinations of semiconductor photocatalysts with various polymers and/or carbon-based nanostructures, such as chitosan,[12] reduced graphene oxide (rGO),[26] polyaniline and nitrogen-doped rGO,[71] carbon nanotubes (CNTs) and graphene,[72] polypyrrole,[73] and polyaniline,[74] have also been investigated. Furthermore, MOF-based heterojunctions, such as zeolitic imidazolate framework-8 (ZIF-8) nanoclusters on g-C_3N_4 nanotubes,[75] have been investigated to combine photocatalytic action of g-C_3N_4 with enhanced CO_2 adsorption of a MOF. In addition, ZIF-8 has also been used in MoO_3/ZIF-8 core-shell nanorods for photocatalytic water purification [Cr(VI) reduction].[76] Finally, we should also note that Janus nanostructures, i.e., nanostructures with surfaces with two distinct properties, can be used in heterogeneous photocatalysis, as described in a recent review.[77]

Heterojunctions generally exhibit better performance compared to single material photocatalysts. Nevertheless, further improvements are still necessary to enhance visible-light absorption and improve charge carrier separation. To achieve this, specific types of heterojunctions, namely, Z-scheme heterojunctions and plasmonic photocatalysts, have been investigated to reduce recombination losses and utilize plasmonic effects, respectively.

2. Z-scheme photocatalysts

While common heterojunction photocatalysts improve the carrier separation and reduce charge recombination losses, it is still difficult to achieve efficient charge separation and strong redox capability simultaneously.[17] In a Z-scheme photocatalyst, as illustrated in Fig. 1, the transfer of electrons from the CB of one material to the valence band (VB) of the other material through an electron mediator ensures a larger difference between oxidation and reduction energy levels compared to a heterojunction.[17,78] Consequently, this type of photocatalyst is particularly promising for water splitting reactions, with a theoretical maximum solar energy conversion efficiency of 40%, which is higher than what can be achieved with single photocatalysts (~30%).[79] The Z-scheme concept is actually not a particularly new idea since it was first proposed in 1979.[9] However, this concept has been attracting a lot more attention recently, with increased interest in photocatalytic fuel generation. For example, one of the important attractions of Z-scheme photocatalysts for water splitting is the possibility of combining the hydrogen evolution photocatalyst and oxygen evolution photocatalyst to achieve higher water splitting efficiency. Liquid Z-scheme systems were demonstrated for water splitting in 2001, followed by the demonstration of a solid-state Z-scheme system for water splitting in 2009.[9] In liquid Z-scheme systems, reversible redox mediators in solution have been commonly used.[17] Common electron mediators in liquid Z-scheme systems are Fe^{3+}/Fe^{2+}, IO_3^-/I^-, and NO_3^-/NO_2^-.[78,79] In addition to these, various cobalt-based organic compounds have been reported,[78,79] as well as transition metal polyoxometalates and vanadate ion shuttle.[79] However, due to backward reactions, low pH tolerance, and light harvesting issues in liquid systems, solid-state Z-scheme catalysts are of significant interest.[17] In a solid-state Z-scheme photocatalyst, conductors (metal or carbon based) can serve as electron mediators.[17] The common conductor mediators include Au nanoparticles, Ag nanoparticles, rGO, and carbon nanotubes (CNTs). In addition, defective metal oxides, for example, Mn vacancies in MnO_2, can provide redox couples, in this case Mn^{3+}/Mn^{4+}.[80] Furthermore, direct Z-scheme photocatalysts where electrons are transferred across the interface between two semiconductors have been reported.[17] Energy band alignment in a direct Z-scheme photocatalyst resembles that of a type-II heterojunction, but the charge carrier transfer pathways are distinctly different in these two structures.[81] In a type-II heterojunction, electrons move from the material with a higher conduction band minimum (CBM) to the one with a lower CBM position, while holes move in the opposite direction, minimizing recombination. However, this results in lower redox ability since the resulting redox levels correspond to a higher position of the valence band maximum (VBM) and lower position of the CBM between the two materials.[81] In a direct Z-scheme heterojunction, the electrons in the material with lower CBM recombine with the holes in the material with higher VBM, resulting in a larger difference between oxidation (lower VBM position) and reduction (higher position of the CBM) energy levels and, consequently, improved redox capability.[81] Compared to conventional Z-scheme photocatalysts, direct Z-scheme photocatalysts have an advantage of simpler structure, as well as lower absorption losses due to the light absorbed in the mediator.[78] It should be noted, however, that there is a possibility for the metallic mediator to contribute to the plasmonic enhancement of photocatalytic activity for a suitably constructed system.

Different material combinations have been reported as Z-scheme photocatalysts to date, such as graphene bridged Ag_3PO_4/Ag/$BiVO_4$,[82] $Ag_2Mo_2O_7$/MoS_2,[83] WO_3/g-C_3N_4,[84] g-C_3N_4/SnS_2,[23] TiO_2/$CuInS_2$,[85] TiO_2/CdS,[86,87] α-Fe_2O_3/g-C_3N_4,[88,89] WO_3/g-C_3N_4,[90] $SrTiO_3$:La, Rh/C/$BiVO_4$:Mo,[91] CdS/RGO/g-C_3N_4,[92] black phosphorus/$BiVO_4$,[93] g-C_3N_4/Ag/MoS_2,[94] g-C_3N_4/nanocarbon/$ZnIn_2S_4$,[95] and MnO_2/monolayer g-C_3N_4 with Mn vacancies.[80] g-C_3N_4 is a particularly popular material for Z-scheme photocatalysts, and a number of different material combinations have been reported.[17] Z-scheme photocatalysts in general have been attracting increasing attention for a variety of applications, including degradation of various pollutants as well as fuel generation (water splitting as well as CO_2 reduction).[78,79] They are among the most promising types of photocatalysts, especially when combined with additional modifications, such as plasmonic materials.

3. Plasmonic photocatalysts

For any of the photocatalyst classes of materials discussed above, it is possible to enhance photocatalytic activity by incorporating metal nanoparticles to utilize plasmonic effects, namely, resonant oscillations of the electrons within a plasmonic nanoparticle.

The plasmonic wavelength of a material is dependent on its dielectric function, as well as size and morphology.[96] Plasmonic effects can be combined with other functions for the metal, for example, in solid Z-scheme photocatalysts.[94] They can also enhance the photocatalytic activity of metal-organic frameworks.[97] The enhancement of the photocatalytic activity by plasmonic nanoparticles can occur by different mechanisms, namely, hot electron injection, localized electromagnetic field enhancement, and plasmon resonance energy transfer (PIRET) from the metal to semiconductor through dipole–dipole interaction.[98] The most common nanoparticles are Ag nanoparticles due to their strong localized surface plasmonic resonance (LSPR),[99] although other metals have also been used for the purpose of plasmonic enhancement. While the use of noble metals (Ag and Au) for this purpose is common,[96,98] there have also been reports on the use of non-noble metals, which has an advantage of lower cost, and the use of more abundant materials. For example, the use of bismuth metal has been reported.[18,100] In addition, Al[96] and Cu[96,101] have also been proposed as suitable candidates for the plasmonic enhancement of photocatalysis since their plasmonic wavelengths can be tuned from 150 nm to 600 nm and from 600 nm to 1000 nm, respectively.[96] Furthermore, non-metallic materials, such as MoS_2, have also been reported.[102] To further tune the properties and achieve increased enhancement, it is possible to use combinations of materials, such as Au/Ag/Cu_2O core-shell nanorods[103] or Au/CuSe/Pt (where CuSe nanosheets and Au provide plasmonic effects, while Pt is a co-catalyst).[104] In addition, the use of connected instead of isolated nanoparticles could lead to an increased electromagnetic field due to strongly coupled structures and, consequently, increased photocatalysis enhancements.[105] Similarly, plasmonic dimers have demonstrated greater enhancement of hydrogen generation and CO_2 reduction compared to non-dimer structures.[60]

III. APPLICATIONS OF PHOTOCATALYSIS

The applications of photocatalysis can be broadly divided into following categories: pollutant degradation, fuel generation, and synthetic chemistry applications. In this review, we will mainly focus on the main environmentally relevant types of applications, namely, pollutant degradation and fuel generation. Pollutant degradation has been demonstrated for a variety of chemical compounds. Disinfection applications can also be broadly defined as pollutant degradation. Photocatalytic fuel generation reactions include hydrogen evolution and CO_2 reduction. In this section, we will discuss these categories of photocatalyst applications.

A. Pollutant degradation

The use of various photocatalysts for pollutant degradation has been extensively explored, with some recent examples summarized in Table I. The problems from material design point of view that need to be solved are the same as in any other photocatalytic application, i.e., efficient photocatalyst should exhibit high light absorption, low recombination of photogenerated charges, and efficient charge transfer to the reactants. While there are numerous examples of the use of photocatalysis for the degradation of various dyes, this type of application is of less interest in modern photocatalysis research, based on the declining number of publications on dye degradation work published in high impact factor journals. Contributing to the declining interest in photocatalytic dye degradation work is declining significance of insights gained into the photocatalytic mechanism from this type of studies. While the dye degradation can be (in theory) justified by the huge amount of dye pollutants discharged by various industries, including textile industry, and while experiments on dye degradation are very simple and straightforward, the lack of new insights into the process, complications in the interpretation of results, and the lack of practicality of application for industrial wastewater treatment have resulted in declining importance of this type of studies. Since the dyes can undergo irreversible transformation through different pathways during the photocatalytic degradation experiment, other characterizations in addition to the loss rate are needed to evaluate the photocatalytic activity of the material.[106] Consequently, other compounds such as phenol have been proposed to compare photocatalytic activities.[106] The investigation of degradation of phenol is sometimes combined with other applications. For example, the degradation of phenol[107] (as well as organic dyes[108]) and hydrogen evolution were demonstrated in photocatalytic fuel cells. In addition to the shift in the interest in the types of pollutants to be degraded, there has also been a shift in the interest in photocatalytic pollutant degradation in general. The development trends of a research field can be estimated from the trends of publications in high impact factor journals (although the journal impact factor is not a measure of the quality of the work, generally this type of journals tends to publish more papers in areas currently considered to be "hot"). We can observe that while the number of total publications on photocatalysis is still growing, the number of papers on photocatalytic degradation in high impact factor journals has definitely declined, as illustrated in Fig. 3. Nevertheless, it is still relevant to discuss some specific types of pollutants, as well as limitations of photocatalysis in water purification and opportunities in air purification.

1. Emerging pollutants

Among different pollutants, the use of photocatalysis for the degradation of emerging pollutants has been attracting increasing attention. In the case of emerging persistent organic pollutants, conventional treatment measures are either insufficiently effective or they simply transfer the pollutant to another phase (from water to sludge, for example), which could cause secondary pollution. It should be noted, however, that while the lack of selectivity of photocatalytic degradation is often listed as an advantage of photocatalysis, this means that emerging pollutants that are often present at very low concentrations (ng/l to μg/l) would likely still persist, while pollutants with higher concentrations will be more significantly degraded. Therefore, photocatalytic degradation of emerging pollutants, if incorporated at all, likely could only be used as a last treatment stage to only remove low concentrations of pollutants, which could not be removed by other methods. Furthermore, it should be noted that the presence of natural organic matter and various anions and cations in the water can affect the overall effectiveness and reaction pathways of photocatalytic degradation of pollutants.[13,15,109] The presence of other species in the water in addition to target pollutants limits the effectiveness of the process by absorbing or scattering light and by scavenging generated reactive oxygen species.[15] Furthermore, there is a possibility of generation of toxic, assimilable, and sensory-unpleasant

TABLE I. Photocatalysts for pollutant degradation. RhB denotes Rhodamine B dye, MO denotes methyl orange dye, MB denotes methylene B dye, BPA denotes Bisphenol A, SMZ denotes Sulfamethazine, TC denotes tetracycline, BP denotes black phosphorus, and QDs denote quantum dots.

Materials	Pollutant	Reaction condition	Irradiation	Reference
N, S doped TiO_2 and N, S doped ZnO	TC	100 ml TC solution (25 mg/l and pH = 7)	6 LED lamps	12
Bi metal@defective BiOCl	NO	0.1 g (60 °C dried) NO (600 ppb) in air	150 W halogen tungsten lamp ($\lambda > 420$ nm)	18
BP/poly-C_3N_4 heterostructure	RhB	20 mg/80 ml RhB solution (10^{-5} mol/l)	300 W Xe lamp ($\lambda > 420$ nm)	20
Ti^{3+}-doped anatase TiO_2	MO	0.1 g/100 ml MO aqueous solution (20 mg/l)	300 W mercury lamp ($\lambda > 400$ nm)	30
Ti-based perovskite nanostructures	TC	50.0 mg in TC aqueous solution	300 W Xe lamp, visible light	31
Black TiO_2 NCs	MB	MB (20 ppm, 100 ml)	Solar light irradiation with a $\lambda > 390$ nm filter	39
g-C_3N_4 nanocapsules	RhB	40 ml RhB solution (1 mg/l)	Visible-light irradiation ($\lambda > 420$ nm)	41
Ultra-thin TiO_2	RhB	40 ml RhB solution (1 mg/l)	300 W Xe lamp (100 mW/cm^2) with an AM 1.5 filter and a cutoff filter	46
Thin film black titania ($H-TiO_{2-x}$)	MB	10 ppm MB solution	55 W Xe lamp	47
N-doped porous carbons	Phenol	50 mg/l, 100 ml phenol solution (200 ppm)		48
Cl intercalated *g*-C_3N_4	RhB	50 mg in 50 ml RhB solution (0.01 mM)	500 W Xe lamp with a $\lambda > 420$ nm filter	52
Cl intercalated in *g*-C_3N_4	NO	NO gas (600 ppb)	150 W lamp with a 420 nm filter	52
MoO_3@ZIF-8 core-shell nanorods	Aqueous Cr (VI)	50 mg in 100 ml of Cr(VI) aqueous solution (20 mg/l)	Solar simulator($\lambda > 440$ nm)	76
SnS_2 with polyaniline and *N*-doped rGO	Aqueous Cr(VI)	300 mg in 300 ml of 50 mg/l $K_2Cr_2O_7$ aqueous solution (pH = 5.3) and 1 ml of methanol	Visible-light ($\lambda > 420$ nm)	71
Ag_2O/Bi_5O_7I	BPA and phenol	50 mg/50 ml of aqueous solution of BPA (20 mg/l) or phenol (20 mg/l)	5 W white LED (400 nm $\geq \lambda \geq$ 800 nm)	63
$CeO_{2-x}AgI$	BPA	30 mg in 60 ml BPA solution (5 mg/l)	300 W Xe lamp with a UV filter, 100 mW/cm^2	61
g-C_3N_4/Bi_2WO_6 2D/2D heterojunction	Ibuprofen	0.2 g/l in 2.5 ml ibuprofen solution (500 μM)	300 W Xe lamp with a 420 nm cutoff filter 326 mW/cm^2	62

TABLE I. (*Continued.*)

Materials	Pollutant	Reaction condition	Irradiation	Reference
$Ag/Ag_3PO_4/BiVO_4/rGO$	TC	50 mg in 100 ml aqueous solution (10 mg/l)	300 W Xe lamp, 100 mW/cm^2 with a 420 nm filter	82
2D/1D MoS_2 nanosheet-decorated $Ag_2Mo_2O_7$	Levofloxacin	1 g/l in 5 ppm levofloxacin in distilled water	150 W Xe lamp with an AM 1.5 G filter	83
$WO_3/g\text{-}C_3N_4$	Antibiotics	50 mg in 100 ml antibiotic solution (25 mg/l)	300 W Xe lamp ($\lambda > 420$ nm)	84
CdS/C_3N_4 with rGO	Atrazine	20 mg in 100 ml atrazine solution (10 mg/l)	350 W Xe lamp with UV and IR filters	92
$g\text{-}C_3N_4/Ag/MoS_2$	RhB	100 mg in 100 ml of RhB solution (20 ppm)	300 W Xe lamp, 172 mW/cm^2 ($\lambda > 420$ nm)	94
$g\text{-}C_3N_4$ with Ag—TiO_2(B) and Au—TiO_2(B) nanorods	RhB/phenol	20 mg in 100 ml RhB/phenol solution (10 mg/l)	250 W visible lamp, $390 \leq \lambda \leq 800$ nm	98
Ag nanoparticles-$\alpha NiMoO_4$	TC	0.1 g in 70 ml aqueous TC solution (20 mg/l)	Visible light	99
Bi metal-C_3N_4 on Bi_2WO_6	MO, RhB, and 2,4-DCP	100 mg in 100 ml aqueous solution (10 mg/l MO, 20 mg/l RhB, 20 mg/l 2,4-DCP)	300 W Xe lamp ($\lambda > 420$ nm)	62
$Au/Ag/Cu_2O$	MO	0.15 mg/ml catalyst dispersed into 10 ml MO solution (50 mg/l)	A 300 W Xe lamp, 71 mW/cm^2 with a UV cutoff filter of $400 < \lambda < 780$ nm	103
$AgI/Bi_{12}O_{17}Cl_2$ heterojunction	SMZ	50 mg in 50 ml aqueous SMZ solution (10 mg/l)	300 W Xe lamp ($\lambda > 420$ nm)	111
Perovskite oxide ultrathin nanosheets/$g\text{-}C_3N_4$ 2D-2D heterojunction	TC	40 mg in 40 ml TC aqueous solution (35 mg/l)	Visible light, 500 W tungsten lamp	114
$Zn_{0.9}Fe_{0.1}S$ on Ni foam	Norfloxacin	(5–20 mg/l) norfloxacin solution	500 W Xe lamp, visible light and 6.1 W/cm^2	115
poly-C_3N_4 foam	TC	50–200 mg in 21 mg/l TC solution	150 W Xe lamp ($\lambda > 420$ nm)	116
$g\text{-}C_3N_4$/carbon QDs/single-atom Ag	Naproxen	50 mg in 50 ml of aqueous naproxen solution (4 mg/l)	350 W Xe lamp and a band-pass filter	120
rGO/silica/zirconia	BPA	0.375 g/l catalyst in 200 ml BPA solution(10 mg/l)	Metal halide lamp (400 W, $\lambda = 400$ nm)	122
N—TiO_2	Microplastic	10 mg, 200 mg extracted microplastics in 30 ml cyclohexane	27 W fluorescent lamp $400 < \lambda < 800$ nm	124
Ag/TiO_2	Organic pollutants and Cr(VI)	0.5 g/l in 300 μM pollutant solution	300 W Xe lamp ($\lambda > 320$ nm)	128

TABLE I. (*Continued.*)

Materials	Pollutant	Reaction condition	Irradiation	Reference
Fe_3O_4@BiOI@AgI	RhB, BPA	30 mg in 60 ml RhB (5 mg/l) or BPA (20 mg/l) aqueous solution	300 W Xe lamp, 100 mW/cm^2 ($\lambda > 400$ nm)	137
Carbon QDs/$ZnFe_2O_4$	NO	0.1 g in 20 ml distilled water	300 W Xe lamp ($\lambda > 420$ nm)	139
$(BiO)_2CO_3/BiO_{2-x}$/graphene	NO	NO, 430 ppb	Simulated solar light irradiation	140
BiOCl/$BiVO_4$/N−graphene QDs	BPA	20 mg in 50 ml BPA solution (10 mg/l)	250 W Xe lamp ($\lambda > 400$ nm)	141
BiOBr/bismuth oxyhydrate photocatalyst	RhB and acetophenone (AP)	100 mg in 200 ml aqueous solution of RhB (15 ppm) or AP (120 ppm)	300 W Xe lamp (385–740 nm) and visible ($\lambda \geq 420$ nm)	142
g-C_3N_4	MO	0.3 g in 100 ml MO aqueous solution (0.4 mg/l)	300 W Xe lamp with a cutoff filter	143
g-C_3N_4/$ZnFe_2O_4$	Cr(VI) and phenol	0.2 g in 20 ml solution (20 ppm $K_2Cr_2O_7$ solution and 20 ppm phenol solution)	300 W Xe lamp ($\lambda > 400$ nm)	74
$ZnFe_2O_4$ decorated mesoporous Al_2O_3 modified MCM-41	Phenol	Phenol solution at pH 6	Sunlight	129
$ZnFe_2O_4$ decorated mesoporous Al_2O_3 modified MCM-41	Cr (VI)	20 mg in 20 ml Cr (VI) (20 ppm) solution	Sunlight	129
$ZnFe_2O_4$/(rGO)	Ciprofloxacin (CIP)	20 mg in 20 ml CIP solution (20 ppm)	Solar	119
$ZnFe_2O_4$	RhB, Congo red	0.02 g/20 ml RhB (5 ppm) or Congo red (10 ppm)	Solar	22
$ZnFe_2O_4$-carbon allotropes	Norfloxacin	20 mg in 20 ml norfloxacin suspension (50 ppm)	Sunlight	118
$ZnFe_2O_4$-carbon allotropes	Cr (VI)	2 ml Cr (VI) solution and 3 M H_2SO_4 solution	Solar	118
p-$CaFe_2O_4$/*n*-$ZnFe_2O_4$	TC and CIP	100 mg in 100 ml antibiotics solution (20 ppm)	125 W, mercury lamp ($\lambda > 420$ nm)	56
CdS QDs and $CaFe_2O_4$@$ZnFe_2O_4$	Norfloxacin	50 mg/l	300 W Xe lamp ($\lambda > 400$ nm)	109
Zinc ferrite/*g*-C_3N_4	Ciprofloxacin	20 ppm	150 W Xe lamp and 1 M $NaNO_2$ as a UV filter	73
Zinc ferrite/*g*-C_3N_4	*Escherichia coli*	100 μl, 20–100 μg/ml	150 W Xe lamp and 1 M $NaNO_2$ as a UV filter; 50 W Xe lamp and 1 M $NaNO_2$ as a UV filter	73

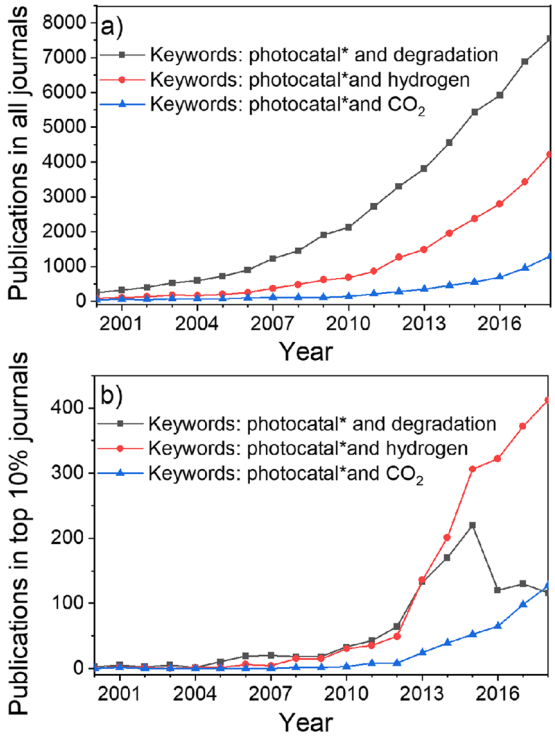

FIG. 3. The number of papers vs year in ISI Web of Science using specified set of keywords for (a) all journals and (b) top 10% journals in materials science (current top journals used for all years).

transformation products if photocatalysis is used for water treatment.[110]

a. Pharmaceuticals. There are different categories of emerging pollutants, including various personal care products, pharmaceuticals, and persistent organic pollutants. Antibiotics belong to the category of emerging pollutants since their extensive use in human, veterinary, and agricultural applications has resulted in contamination of surface, ground, and drinking water.[82,99,111,112] Pharmaceutical factories and hospital wastewater could also contribute to the presence of pharmaceuticals in water.[99,113] In the environment, antibiotics can form unknown complex mixtures with other organic pollutants or heavy metals, affect the biological organisms in the environment, and contribute to the increase in antibiotic resistant infections.[83] They are typically not completely removed during the standard wastewater treatment process but can be removed by photocatalysis. It has been shown that photocatalytically treated antibiotic contaminated water did not promote antibacterial resistance over a period of one year.[113] Various photocatalysts have been proposed for the degradation of antibiotics, such as Ag_3PO_4/Ag/$BiVO_4$ Z-scheme photocatalysts,[82] g-C_3N_4/$K^+Ca_2Nb_3O_{10}^-$,[114] doped porous carbon nitride,[111] AgI/$Bi_{12}O_{17}Cl_2$,[112] $Ag_2Mo_2O_7$/MoS_2 Z-scheme 1D/2D photocatalysts,[83] α-$NiMoO_4$ nanorods/Ag nanoparticle plasmonic photocatalysts,[99] doped ZnO and TiO_2 composites with chitosan,[12] $Zn_{0.9}Fe_{0.1}S$/Ni foam,[115] polymeric carbon nitride,[116] p-$CaFe_2O_4$/n-$ZnFe_2O_4$,[56] CdS QDs/$CaFe_2O_4$/$ZnFe_2O_4$,[109] WO_3/g-C_3N_4 Z-scheme photocatalysts,[84] BiOCl/g-C_3N_4/Cu_2O/Fe_3O_4,[117] polypyrrole sensitized zinc ferrite/graphitic carbon nitride,[73] $ZnFe_2O_4$/carbon derivatives,[118] and $ZnFe_2O_4$/rGO.[119] In some cases, both antibiotic pollutant degradation and hydrogen evolution have been demonstrated.[116] In addition to antibiotics, the degradation of other pharmaceuticals and personal care products is also of significant interest.[120,121] For example, the degradation of naproxen, a common non-steroidal anti-inflammatory drug, was demonstrated using a photocatalyst consisting of g-C_3N_4, carbon quantum dots, and single-atom dispersed silver.[120] Another carbon nitride based heterojunction photocatalyst has also been demonstrated to effectively degrade ibuprofen.[62] In addition, TiO_2 was shown to be effective for the degradation of carbamazepine, diclofenac, and ibuprofen in a reactor using visible LEDs as the light source.[121]

b. Plastics industry pollutants—endocrine disruptors and microplastics. Another class of emerging pollutants of significant interest are endocrine disruptors, such as bisphenol A, which is commonly used in epoxy resins and polycarbonate plastics.[122] Different materials have been proposed for bisphenol A degradation, such as CeO_2—AgI,[61] cyclodextrin decorated TiO_2 spheres,[123] Ag_2O/Bi_5O_7I,[63] and reduced graphene oxide (rGO) supported on silica and zirconia.[122] Microplastics represent another class of emerging pollutants that are a significant concern due to their persistence in the environment. They originate from primary sources, i.e., micrometer-sized plastics discharged into the environment such as high density polyethylene particles from personal care products, and secondary sources, i.e., from breakdown of larger plastics pieces.[124] Some promising results on microplastic degradation using photocatalysis have been reported, but overall the number of publications is low. The materials that have been reported to be effective for microplastic degradation include nitrogen-doped TiO_2[124] and ZnO.[125] It should be noted that the demonstration of photocatalytic degradation of microplastics is relatively recent compared to the research on other emerging pollutants, although it has been known that the incorporation of photocatalytic particles (ZnO or TiO_2) into plastics can affect their weathering under UV illumination.

2. Limitations for practical applications in water purifications

It should be noted that even for emerging pollutants, it is likely that the practical applications of photocatalysis will face the same problems as the applications in conventional wastewater treatment.[126] In simple terms, the biggest issues with practical applications of photocatalysis are problems with scaling up to an industrial process and being cost-effective and time-effective.[126] Despite the fact that photocatalysis has been around for almost half a century, so far there is only one commercial photocatalytic water treatment system, the Purifics Photo-Cat.[126] The system is not solar, but rather it uses UV lamps, and its efficiency can actually be higher if the photocatalyst is replaced with hydrogen peroxide dosing.[126] In addition, while a suspended photocatalyst reactor, i.e., the same type as used in the Purifics Photo-Cat, is the most viable and practical option, the treatment cost is further increased by photocatalyst recovery in this design.[14,126] Furthermore, while visible-light photocatalysis is a very popular topic among photocatalysis research papers, it should

be noted that using solar energy instead of UV lamps would require much higher land area footprint, with basically two order of magnitude larger area needed to provide the same light energy (and that would apply only for a small part of the day and optimal weather).[126] Generally, photocatalytic water treatment systems are considered impractical in the water treatment industry since conventional technologies exhibit significantly higher energy efficiency.[15] Conventional advanced oxidation processes involving the use of ozone, chlorine, and/or hydrogen peroxide with or without UV irradiation typically have electrical energy per order values E_{EO} (energy in kW h required to degrade the contaminant by one order of magnitude in 1 cubic meter of contaminated water) below 1 kW h/m^3, while for UV photocatalysis this value exceeds 100 kW h/m^3.[127] Thus, it is unrealistic to expect significant changes in the application of photocatalysts in industrial water treatment. Niche applications have been proposed as a possible way forward, and these include applications to specific pollutants, such as heavy metal reduction to a less toxic or less soluble form [Cr(VI) to Cr(III)[15,71,74,76,118,128,129] and U(VI) to U(IV)[130]] and smaller scale applications.[15]

3. Pathogen elimination

Photocatalysis can also be applied for water disinfection, and it is effective not only against bacteria[131] but also against viruses.[132] For a detailed review of antimicrobial activity of photocatalysts, see Ref. 133. Consequently, solar photocatalysis is often cited as a possible solution for ensuring safe drinking water supply in the developing countries. While the main challenge in the developed countries is the maintenance of existing infrastructure and the treatment of wastewater, in developing countries, the priority is obtaining safe drinking water by eliminating pathogenic microorganisms.[134] Similar to water treatment for pollutant removal, despite successes in lab-scale experiments, industrial scale photocatalytic disinfection is impractical. For example, various pilot photocatalysis projects, such as the Solwater TiO_2/solar concentrator project, have confirmed unrealistic treatment times and volumes (4 h for disinfection in a 20 l reactor).[126] There are considerably more cost-effective solutions, which use solar energy and are applicable to the developing countries, such as solar pasteurization and solar disinfection (SODIS).[134,135] SODIS, in particular, provides a solution that is difficult to beat in terms of simplicity and low cost—it simply involves filling water into transparent containers such as plastic bottles with one side painted black (or alternatively they can be placed on a black surface) and leaving them out in the sun for a period of time.[134] The method can be improved by using parabolic concentrators and glass containers, which can shorten treatment time and eliminate the need for periodic replacement of plastic bottles.[134] While on the lab-scale improvements in SODIS by photocatalyst incorporation have been demonstrated, there have been no practical field designs due to difficulties and drawbacks for both suspended and immobilized photocatalyst reactors.[136] Therefore, the usefulness of photocatalysis for practical disinfection applications is limited. However, the investigation of the toxicity mechanisms of photocatalysts from the basic science point of view could still be potentially interesting since the mechanisms of action are still not well understood.[131] This includes the fact that antibacterial activity and photocatalytic pollutant degradation can proceed based on different pathways[61,137] and can exhibit different trends, i.e., efficient antibacterial materials are not necessarily good for pollutant degradation and vice versa.

4. Air purification

Finally, in addition to water treatment, photocatalysis could be applied to air treatment.[138–140] The pollutants of interest include NO_x, SO_x, CO, H_2S, and volatile organic compounds (VOCs).[138] It has been proposed that different from water treatment and fuel generation, photocatalysis can be both economically and technologically competitive for air treatment.[138] For a detailed review of this application, see Ref. 138.

B. Fuel generation

Photocatalytic fuel generation includes photocatalytic water splitting to produce hydrogen and photocatalytic CO_2 reduction to produce hydrocarbon fuels. As all photocatalytic processes, photocatalytic fuel generation reactions involve light absorption, followed by separation and transport of charge carriers, and finally surface redox reaction, in this case the reduction of water or CO_2 by photogenerated electrons.[7] For efficient redox reactions, however, it is necessary for the energy band positions (valence band for oxidation reaction by holes and conduction band for reduction reaction by electrons) to match the oxidation and reduction potentials of water splitting and the reduction potential of CO_2.[7] The number of potential photocatalysts that can produce hydrogen from water (conduction band more negative than the redox potential of H_2/H_2O and valence band more positive than the redox potential of O_2/H_2O) is limited, as illustrated in Fig. 4.[7] Similarly, for CO_2 reduction, the conduction band edge needs to be more negative than the corresponding redox potential.[7] Furthermore, reactants should be adsorbed onto the photocatalyst, while reaction products should desorb, and excess opposite charge carriers, such as holes in the carbon dioxide reduction process, should be scavenged before they recombine with photogenerated electrons.[6] While charge separation is typically addressed by photocatalyst design (heterojunctions and Z-scheme photocatalysts), attention should also be devoted to reactor design to separate reaction products to prevent back reactions.[6] For the CO_2 reduction, aqueous photoreactors and gas-phase photoreactors can be used.[6]

Both water splitting and CO_2 reduction reactions are "uphill" chemical reactions, resulting in an increase in the Gibbs free energy. Therefore, for both types of reactions, the biggest problem is the low efficiency of the process. However, hydrogen production by water splitting is a simple reaction and a two electron process. In contrast, CO_2 reduction is complex and requires 6–8 electrons, with a range of possible reaction products.[6,7] Consequently, due to increased complexity of reactions, the efficiency of CO_2 reduction is even lower than that of hydrogen production.[7] Unfortunately, from the point of view of mitigating climate change, CO_2 reduction is more attractive since it can generate hydrocarbon or alcohol fuels from CO_2. Consequently, the photocatalysis research into fuel generation has been rapidly developing. Several detailed reviews of CO_2 reduction[6] and hydrogen production[9] have been published recently. A particularly attractive concept in solar fuel generation is the artificial photosynthesis,[6] where useful fuels can be generated from carbon and water. Unlike natural photosynthesis, which produces carbohydrates, artificial photosynthesis produces a range of partially reduced compounds, such as CO, CH_4, and methanol.[26] The most common products of CO_2 reduction are carbon monoxide and methane. Photocatalytic CO_2 reduction rarely results in high-grade carbon species

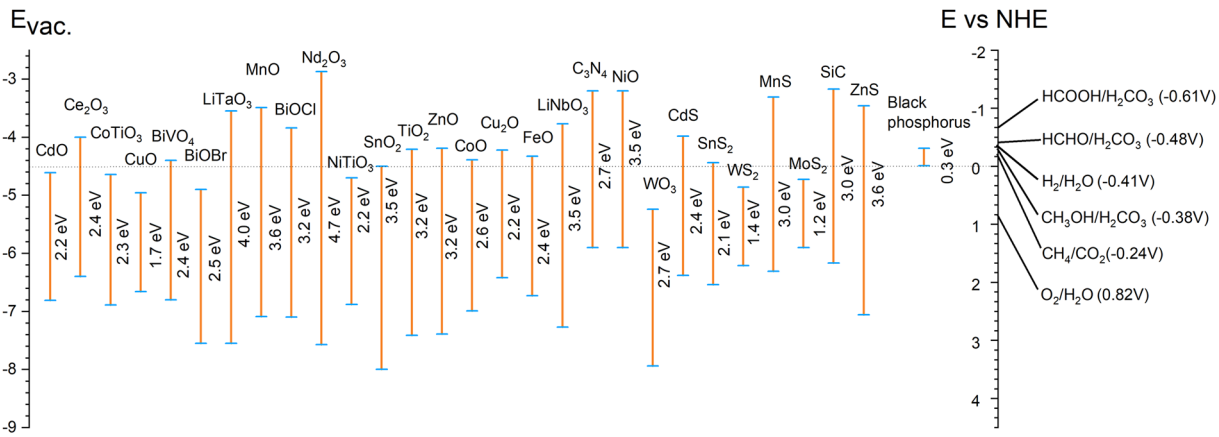

FIG. 4. Band edge positions of different photocatalysts relative to various redox potentials at pH = 7. The band edge positions according to Refs. 141–143, 168, 170, and 194–196.

(C_n, $n \geq 2$), but, nevertheless, such complex processes are possible.[144] For example, the evolution of CH_4 and C_2H_6 on Au@TiO_2 yolk-shell hollow spheres is illustrated in Fig. 5.[144] It can be observed that while Au@TiO_2 results in the evolution of C_2H_6, TiO_2 alone (including standard photocatalyst P25) does not generate high-grade carbon species, and the generation of C_2H_6 was attributed to the plasmonic enhancement of the electric field by Au nanoparticles within titania shells.[144] Due to significant interest in the generation of high-grade carbon species, the improvement of understanding of the processes involved in producing C_n, $n \geq 2$, carbon species is crucial for the development of high performance photocatalysts for solar fuel generation.

Both reactions also utilize similar photocatalyst materials since the values of redox potentials for CO_2 and H_2O reduction are close[28] and tend to use co-catalysts. Nanoparticle co-catalysts (most commonly, noble metals) are used to provide active sites and reduce activation energy for the reaction.[145] In addition to increasing the activity, co-catalysts can also affect the charge separation, selectivity, stability, and back reactions.[69] Co-catalysts commonly promote either reduction or oxidation reactions, such as hydrogen evolution reaction (HER) or oxygen evolution reaction (OER) in water splitting. However, they can also increase the rates of backward reactions, for example, hydrogen oxidation reaction (HOR) and oxygen reduction reaction (ORR) in water splitting. Therefore, an important part of the design of the photocatalytic water splitting system is the selective deactivation of reverse reactions. For example, the use of oxides of Ni, Ir, and Ru instead of pure metals suppresses ORR while retaining the promotion of HER and OER.[9] Although there have been examples of co-catalyst-free fuel generation photocatalysts,[146] the majority of reported photocatalysts for both water splitting and CO_2 reduction include some form of co-catalysts. Co-catalysts can be classified as noble metal and rare earth co-catalysts, noble-metal-free

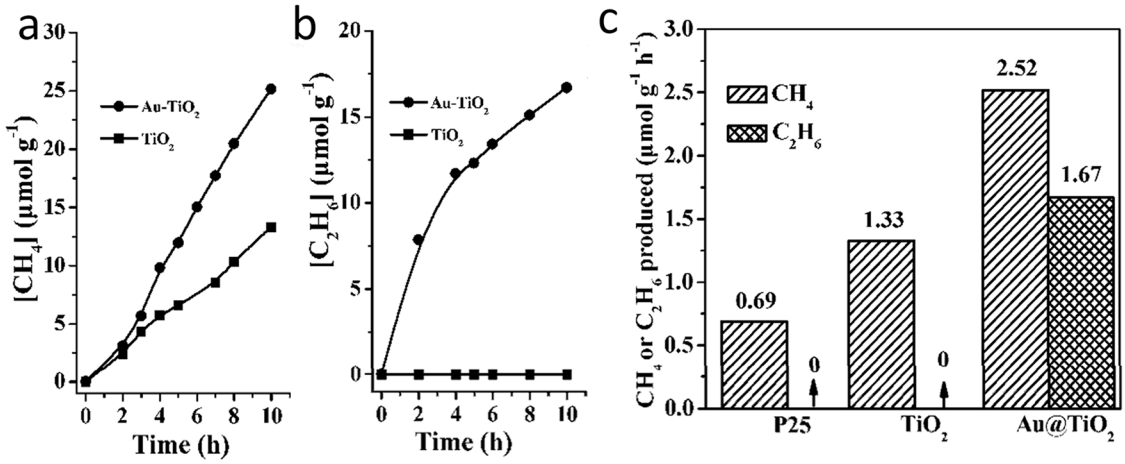

FIG. 5. (a) CH_4 and (b) C_2H_6 evolution amounts and (c) comparison of photocatalytic activity for CO_2 reduction over P25, TiO_2 hollow spheres, and Au@TiO_2 yolk-shell hollow spheres. Reproduced with permission from Tu *et al.*, Nanoscale **7**, 14232–14236 (2015). Copyright 2015 The Royal Society of Chemistry.

co-catalysts, metal-free co-catalysts, and biological co-catalysts.[69] For a detailed review of co-catalysts for CO_2 reduction, see Ref. 69. Noble-metal co-catalysts are very commonly used for both water splitting and CO_2 reduction. Various co-catalysts used in recent works include Pt as the most common co-catalyst,[41,49,88,90,147–149] as well as Cu^I/Pd,[33] Ru,[91] Pd,[54] and Rh.[54] Noble metals combined with metal oxides could also be used as co-catalysts, such as Au—TiO_2.[150] However, due to high cost and scarcity of noble metals and rare earths, possible alternatives are the use of single-atom catalysts, which are generally promising for photocatalytic applications,[151–154] or the development of non-noble-metal co-catalysts. For a detailed review on single metal atom photocatalysis, see Ref. 153. It should be noted that non-noble metals can also serve as single-atom co-catalysts,[155] although non-noble-metal materials are more commonly investigated in other forms, and 2D materials and clusters are of significant interest in addition to single-atom catalysts.[156] For example, 2D materials, such as MoS_2, can serve as effective co-catalysts due to abundant active sites at edges.[65] Other metal sulfides have also been reported to be effective co-catalysts, such as CoS_x polyhedrons.[4] Other non-noble-metal co-catalysts have also been reported, such as amorphous NiO,[66] Co_2P,[157] $Co(bpy)_3^{2+}$ (bpy = 2′,2 bipyridine),[70] and MnO_x,[150] as well as metal-free co-catalysts, such as phosphorene,[69] Ti_3C_2 MXene,[158] and graphene oxide.[159] In addition, dual co-catalysts, such as NiS/carbon dots,[160] CoP, and Pt[161] have been reported. Dual co-catalysts can enable the enhancement of both oxidation and reduction reactions, but co-loading of different types of co-catalysts has been less explored to date.[9,162] In addition to co-catalysts, some research works report the use of photosensitizers, such as Ru-based dye.[55] It should also be noted that the reactions are typically affected not only by the material choice for the co-catalyst but also by the co-catalyst size and morphology.[163,164] Both efficiency and selectivity can be affected by co-catalyst size and morphology since these factors (size and terminating facets) determine the concentrations and types of active sites present on the surfaces.[163,164]

Another feature that both reactions have in common is that reports in the literature often involve half-reactions, with sacrificial agents and/or electron donors added.[9,165] However, it should be noted that sacrificial half-reactions are generally "downhill" chemical reactions, different from true water splitting and/or CO_2 reduction, which are uphill processes.[9] Consequently, photocatalytic activities for true water splitting and sacrificial reactions are not directly correlated.[9] Furthermore, since the common sacrificial donors, such as alcohols and triethanolamine, contain carbon and hydrogen, they can contribute to the measured yield of reaction products and result in erroneous estimations of yield.[165] Despite the calls for improved reporting on heterogeneous photocatalysis and summaries of best practices,[165,166] the majority of literature reports still use sacrificial agents and only investigate the reduction part of the reaction. For a more detailed discussion of overall water splitting, see Ref. 166.

C. Water splitting and/or hydrogen evolution reaction

Photocatalysts reported for water splitting/HER include various metal oxide and oxynitride nanosheets;[145] g-C_3N_4 and various CN forms;[49,147] CdS/MoS_2 core-shell nanowires; black phosphorus/g-C_3N_4;[167] α-Fe_2O_3/g-C_3N_4 Z-scheme photocatalysts;[88] NiO/g-C_3N_4;[66] ZnS//g-C_3N_4;[67] g-C_3N_4/$ZnIn_2S_4$;[68] NiS/carbon dots/CdS;[160] phosphorene/g-C_3N_4;[69] CoS_x/g-C_3N_4;[4] multiwalled carbon nanotube (MWCNT)/graphene/TiO_2;[72] WO_3/g-C_3N_4;[90] MoS_2/TiO_2;[102] $SrTiO_3$:La, Rh/C/$BiVO_4$:Mo Z-scheme photocatalysts;[91] g-C_3N_4/TiO_2;[148] g-C_3N_4/Co_2P;[157] CdS/RGO/g-C_3N_4;[92] Ti_3C_2 MXene on CdS, ZnS, or $Zn_xCd_{1-x}S$;[158] black phosphorus/$BiVO_4$;[93] g-C_3N_4/Ag/MoS_2;[94] black phosphorus[21] multishell g-C_3N_4;[41] Ag dimer/$ZnIn_2S_4$ nanosheets/TiO_2 nanofibers;[60] g-C_3N_4 co-modified with MnO_x and Au—TiO_2;[150] and boron-doped g-C_3N_4/anatase titania nanocomposites,[146] as summarized in Table II. Carbon nitrides are commonly used in water splitting,[168] despite the drawbacks of low rates of hydrogen and especially oxygen evolution, which can be somewhat improved by using metal co-catalysts and sacrificial electron donors or acceptors (i.e., investigating half-reactions instead of the full process).[27] For a detailed review of g-C_3N_4 photocatalysts, see Ref. 168.

It should be noted that when discussing progress made to date, due to the fact that reaction rates are strongly dependent not only on the photocatalyst used but also on the actual experimental conditions used for photocatalytic activity testing, it is not possible to provide meaningful comparisons of the numbers reported in different studies. We, therefore, simply list some examples of relevant materials and discuss important issues for the commonly investigated ones. We will also list some recent achievements in terms of apparent quantum yield (AQY) or apparent quantum efficiency (AQE) since the information on AQY or solar-to-hydrogen (STH) efficiency provides some basis for comparison in water splitting applications.[168] Among few studies that report apparent quantum efficiency for water splitting, reported figures include the following AQEs at 420 nm (unless stated otherwise): 27.8% on mesoporous N-doped g-C_3N_4,[49] 28.5% on CdS/MoS_2 core-shell nanowires, 57% (with NaCl) on polymeric CN with shorter interlayer distance,[169] 8.57% on crystalline CN nanosheets,[147] 44.35% on α-Fe_2O_3/g-C_3N_4 Z-scheme photocatalysts,[88] <0.1% for NiO/g-C_3N_4,[66] 7.05% for g-C_3N_4/$ZnIn_2S_4$ nanoleaf,[68] 19% on $SrTiO_3$:La, Rh/C/$BiVO_4$:Mo,[91] 36.5% on CdS/RGO/g-C_3N_4,[92] 0.89% on black phosphorus/$BiVO_4$,[93] and 2.78% on g-C_3N_4 co-modified with MnO_x and Au—TiO_2.[150] The exceptionally high AQY of polymeric CN prepared by co-condensation of urea with oxamide in molten salt (KCl/LiCl) mixture was attributed to reduced interlayer stacking and extended visible-light absorption, which resulted in increased generation of dissociated surface charge carriers that could participate in photocatalytic reactions.[169] The XRD patterns of CN samples prepared under different conditions, high resolution TEM image of the optimized sample, and proposed scheme for interlayer charge transfer are shown in Fig. 6, where decreased interlayer spacing can be clearly observed. It can, thus, be observed that there is a huge variation in values reported for different materials, and despite the fact that AQE/AQY values provide at least some basis for performance comparisons, it would be highly beneficial to the progress of the field to standardize the experimental conditions (reactor geometry, illumination, and additives if any).

D. CO_2 reduction

A number of different photocatalysts for CO_2 reduction have also been reported,[6] and various synthetic methods for their preparation have been recently reviewed.[171] Various photocatalysts

TABLE II. Summary of literature reports on H_2O splitting/HER. BP denotes black phosphorus, NS denotes nanosheet, TEOA denotes triethanolamine, and NC denotes nanocarbon.

Materials	Reaction condition	Irradiation	Efficiency	Reference
BP NS	5 mg in 100 ml aqueous solution, 0.75 m Na_2S, and 1.05 m Na_2SO_3	300 W Xe lamp ($\lambda > 420$ nm), 0.255 J/s	512 μmol h^{-1} g^{-1}, QE = 0.47%	21
Ti^{3+}-doped anatase TiO_2	0.1 g in 90 ml deionized water, 10 ml methanol, and 0.5 ml of 1 wt. % Pt co-catalyst	UV/visible ($\lambda > 400$ nm)	16.65 μmol h^{-1} g^{-1}, visible light	30
Nitrogen deficient g-C_3N_4	10 mg in 25 vol. % aqueous lactic acid solution and 1 wt. % Pt co-catalyst	300 W Xe lamp ($\lambda > 420$ nm)	6.9 $mmol^{-1}$ g^{-1}	35
Porous nitrogen-defective C_3N_4	10 mg in 150 ml aqueous solution with 10 vol. % methanol and 1 wt. % Pt co-catalyst	300 W Xe lamp ($\lambda > 400$ nm)	1 160 μmol h^{-1} g^{-1}	36
Porous defective modified g-C_3N_4	50 mg in 80 ml aqueous solution with 10 vol. %TEOA and 3 wt. % Pt co-catalyst	300 W Xe lamp ($\lambda > 420$ nm)	AQE_{420nm} = 8.41%, 334.2 μmol H_2 in 5 h	37
g-C_3N_4 thin NS	100 mg in 100 ml of 20 vol. %aqueous lactic acid solution and 1 wt. % Pt co-catalyst	300 W Xe lamp ($\lambda > 420$ nm), 200 mW	99.1 μmol h^{-1}	40
g-C_3N_4 nanocapsules	40 mg, 10 ml TEOA, 80 ml water, 3 wt. % Pt co-catalyst	300 W Xe lamp ($\lambda > 420$ nm)	630 μmol h^{-1} g^{-1}	41
Surface defective anatase TiO_2 NS	30 mg in 80 ml DI water, 20 ml methanol, and 1 wt. % Pt co-catalyst	UV 365 nm	41.04 mmol h^{-1} g^{-1} and QE = 41.6%	44
3D mesoporous ultrathin g-C_3N_4	50 mg in 100 ml of 20 vol. % aqueous lactic acid solution and 1 wt. % Pt co-catalyst	300 W Xe lamp ($\lambda > 420$ nm)	3579 μmol h^{-1} g^{-1} and AQE_{420nm} = 27.8%	49
Na-doped g-C_3N_4	50 mg in 80 ml aqueous solution of 10 vol. %TEOS and 1 wt. % Pt co-catalyst	350 W Xe lamp ($\lambda > 400$ nm)	18.7 μmol h^{-1}	51
Cl intercalated in g-C_3N_4	50 mg in 20 ml water with 10 ml lactic acid and 3 wt. % Pt co-catalyst	300 W Xe lamp ($\lambda > 420$ nm)	537.1 μmol g^{-1} h^{-1} and AQY_{420nm} = 11.9%	52
One-dimensional CdS@MoS_2 core-shell nanowires	20 mg in 80 ml aqueous solution and 8 ml lactic acid	300 W Xe lamp ($\lambda > 420$ nm)	493.1 μmol g^{-1} h^{-1} and AQY_{420nm} = 28.5%	65
Amorphous NiO/g-C_3N_4	50 mg in 100 ml aqueous solution of TEOA (10 vol. %)	300 W Xe lamp, $\lambda > 420$ nm, 1.75 W/cm^2	68.8 μmol g^{-1} h^{-1}	66

TABLE II. (*Continued.*)

Materials	Reaction condition	Irradiation	Efficiency	Reference
ZnS/*g*-C_3N_4	50 mg/400 ml aqueous solution (Na_2S and Na_2SO_3)	300 W Xe lamp ($\lambda > 420$ nm)	713.68 μmol h^{-1} g^{-1}	67
2D/2D *g*-C_3N_4 NS/$ZnIn_2S_4$	50 mg in 50 ml aqueous solution and 10 ml TEOA	300 W Xe lamp ($\lambda > 420$ nm)	2.78 mmol h^{-1} g^{-1} and AQY_{420nm} = 7.05%	68
2D/2D Phosphorene/ *g*-C_3N_4	20 mg in 60 ml water and 20 ml lactic acid	300 W Xe lamp ($\lambda > 400$ nm)	571 μmol/(h g) and AQY_{420nm} = 1.2%	69
V_{Mn}:MnO_2 monolayer/ *g*-C_3N_4	3 wt. % Pt co-catalyst, 10 mg in 50 ml water, 10 ml TEOA, and 20 mg in 100 ml water	300 W Xe lamp ($\lambda > 400$ nm)	28.0 mmol g^{-1} h^{-1} and AQY_{420nm} = 23.33%; H_2:O_2, 2:1 60.6: 28.9 μmol h^{-1} g^{-1}	80
g-C_3N_4/WO_3	Pt co-catalyst, 50 mg in 80 ml aqueous solution (10 vol. % TEOA)	300 W Xe lamp	3.12 mmol h^{-1} g^{-1}	90
CdS/C_3N_4 with rGO	20 mg in water (45 ml) and lactic acid (5 ml)	350 W Xe lamp solar simulator ($400 < \lambda < 800$ nm)	473.4 μmol h^{-1} g^{-1} (AQE = 24.8%)	92
g-C_3N_4/Ag/MoS_2	100 mg in 100 ml of aqueous solution and 15 vol. % of triethanolamine (TEOA)	350 W Xe lamp ($\lambda > 420$ nm)	10.40 μmol h^{-1}	94
g-C_3N_4/NC/$ZnIn_2S_4$	50 mg in 80 ml aqueous solution 0.5M Na_2S and 0.5M Na_2SO_3; 6 °C	12 W UV-LED (λ = 420 nm)	50.32 μmol h^{-1}	95
Cu-TiO_2	1 g/l, methanol/water mixture (volume ratio 1:5)	1000 W Xe lamp ($\lambda \geq 420$ nm)	150 μmol J^{-1} g^{-1}	101
MoS_2/TiO_2	15 ml mixed solution (water and methanol, 8:2 by volume)	300 W Xe lamp and AM 1.5 solar	84 μmol h^{-1}	102
Au-chain@$Zn_xCd_{1-x}S$ (x = 0.67)	0.1 g in 100 ml aqueous solution 0.35M Na_2S+0.25M Na_2SO_3	300 W Xe lamp ($\lambda \geq 420$ nm)	16 420 μmol h^{-1} g^{-1} AQE_{420nm} = 54.6%	104
Tri-s-triazine-based crystalline C_3N_4 NS	3 wt. % Pt co-catalyst and 50 mg in 100 ml solution containing 10 ml methanol	Monochromatic LED	AQY_{420nm} = 8.57%	147
BP/*g*-C_3N_4	1.5 mg in 5 ml methanol:water (1:4 by volume)	320 W Xe lamp, 420 nm < λ < 780 nm, 0.3 W/cm^2	427 μmol h^{-1} g^{-1}	167
NiS/carbon dots/CdS	100 mg in 100 ml aqueous solution (0.25M Na_2S + 0.35M Na_2SO_3)	350 W Xe lamp ($\lambda > 420$ nm)	1444.5 μmol h^{-1} g^{-1}	160
Nanostructured *g*-C_3N_4/TiO_2	0.1 g in 100 ml aqueous solution (10 vol. % TEOA) and 3 wt. % Pt co-catalyst	300 W Xe lamp ($\lambda > 420$ nm)	513 μmol g^{-1} h^{-1}, AQY_{420nm} = 0.15%	148

TABLE II. (*Continued.*)

Materials	Reaction condition	Irradiation	Efficiency	Reference
g-C_3N_4 NS—Co_2P Co-catalyst	50 mg in 80 ml aqueous solution K_2HPO_4 (68 ml distilled water and 12 ml TEOA)	300 W Xe lamp	27.81 μmol h^{-1}	157
Ti_3C_2 MXene co-catalyst	20 mg in 80 ml aqueous solution with 20 ml lactic acid	300 W Xe lamp ($\lambda > 420$ nm)	14 342 mmol h^{-1} g^{-1} and AQY_{420nm} = 40.1%	158
B:g-C_3N_4/TiO_2	0.1 g in 80 ml H_2O and 20 ml methanol	300 W Xe lamp ($\lambda > 420$ nm)	AQE_{420nm} = 3.08%	146
poly-C_3N_4	3 wt. % Pt co-catalyst, 50 mg in 50 ml aqueous TEOA (10 vol. %)	50 W LED, white, blue, and green	AQY_{420nm} = 57% and AQY_{525nm} = 10%	169
2D-2D BP/MoS_2	10 mg in 250 ml aqueous solution (0.1M Na_2S and 0.1M Na_2SO_3)	300 W Xe lamp ($\lambda > 420$ nm s)	1286 μmol h^{-1} g^{-1} and AQY_{420nm} = 1.2%	170
polypyrrole:Zinc ferrite/ g-C_3N_4	20 mg in 20 ml of 10% of methanol aqueous solution	150 W Xe lamp, visible	567 μmol h^{-1}	73

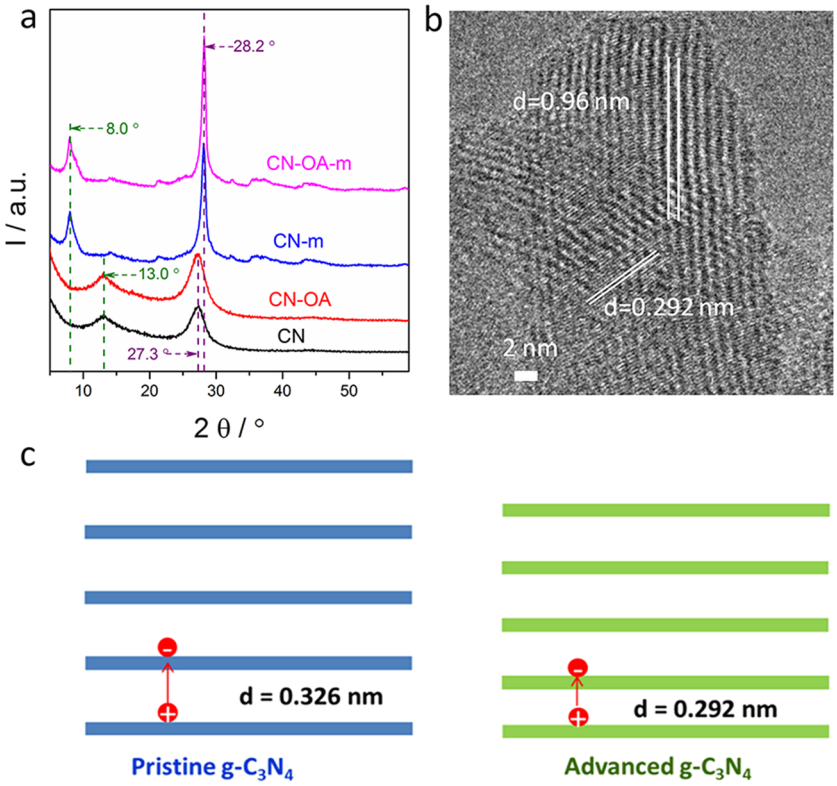

FIG. 6. (a) Powder XRD patterns of CN, CN—OA, CN—m, and CN—OAm. (b) HR-TEM image of CN—OA—m. (c) Proposed interlayer charge carrier transfer of (left) pristine CN (d = 0.326 nm) and (right) optimized CN—OA—m with shortened layer stacking distance (d = 0.316 nm). Reproduced with permission from Zhang *et al.*, Angew. Chem., Int. Ed. **56**, 13445–13449 (2017). Copyright 2017 John Wiley and Sons.

TABLE III. Summary of literature reports on CO_2 reduction. NP denotes nanoparticles, and RT denotes room temperature.

Materials	Reaction condition	Irradiation	Evolution rate/ yield/TCEN/AQY/AQE	Reference
g-C_3N_4/SnS_2	Gas phase	A 300 W Xe lamp ($\lambda \geq 420$ nm)	Methanol, 2.24 μmol g^{-1}; CH_4, 0.64 μmol g^{-1}	23
$CsPbBr_3$ perovskite QD/GO composite	In ethyl acetate	100 W Xe lamp and an AM 1.5 G filter	CO, 58.7 μmol h^{-1} g^{-1}; CH_4, 29.6 μmol h^{-1} g^{-1}; TCEN = 357.4 μmol g^{-1}	26
V_{Bi}-BiBrO ultrathin nanosheets	30 mg in 50 ml water without additives and 0.08 MPa CO_2	300 W Xe lamp	CO, 20.1 μmol h^{-1} g^{-1}	32
Ti^{3+}—TiO_2	Gas phase and Cu^I/Pd co-catalyst	Xe lamp (300 W) (>400 nm)	CH_4, ~1 μmol h^{-1} g^{-1}	33
g-C_3N_4 nanosheets	Gas phase	300 W Xe lamp	Methanol, 1.87 μmol g^{-1} h^{-1}; CH_4, 1.39 μmol g^{-1} h^{-1}	42
O-doped g-C_3N_4	Gas phase	350 W Xe lamp and a 420 nm filter	Methanol, 0.88 μmol h^{-1} g^{-1}	50
Cl intercalated in g-C_3N_4	0.05 g photocatalyst with 1.3 g $NaHCO_3$, 5 ml H_2SO_4 (4M) added to produce 1 atm CO_2 gas	300 W Xe lamp and a filter ($\lambda > 420$ nm)	CO, ~10 μmol h^{-1} g^{-1}	52
g-C_3N_4 nanotubes with ZIF-8 nanoclusters	Gas phase	300 W Xe lamp	CH_3OH, 0.75 μmol h^{-1} g^{-1}	75
N-doped carbon@$NiCo_2O_4$ double-shelled nanoboxes	H_2O/acetonitrile mixture, 30 °C, 1 atm CO_2, with $[Ru(bpy)_3]Cl_2$ $6H_2O$ and triethanolamine (TEOA)	300 W Xe lamp and a 420 nm cutoff filter	CO, 26.2 μmol h^{-1}; H_2, 3.4 μmol h^{-1} and AQY_{420nm} = 1.07%	55
In_2S_3—$CdIn_2S_4$	H_2O/acetonitrile mixture, 30 °C, 1 atm CO_2, with $Co(bpy)_3^{2+}$ and TEOS	($\lambda \geq 400$ nm)	CO, 825 mol h^{-1} g^{-1}	64
$ZnIn_2S_4$—In_2O_3	H_2O/acetonitrile mixture, with $Co(bpy)_3^{2+}$ and TEOS	300 W Xe lamp ($\lambda \geq 400$ nm)	3075 μmol h^{-1} g^{-1}	70
$CuInS_2$/TiO_2	Gas phase	350 W Xe lamp and simulated solar	CH_4, 2.5 μmol h^{-1} g^{-1}; CH_3OH, 0.86 μmol h^{-1} g^{-1}	85
TiO_2/CdS	Vapor phase	300 W Xe lamp	CH_4, 11.9 mmol h^{-1} m^{-2}	87
α-Fe_2O_3/g-C_3N_4	Gas phase and RT	Xe lamp, 0.21 W/cm^2	CO, 27.2 μmol g^{-1} h^{-1}	89
Au@TiO_2 yolk-shell hollow spheres	Gas phase	300 W Xe lamp	CH_4, 2.52 μmol g^{-1} h^{-1}; C_2H_6,1.67 μmol g^{-1} h^{-1}	144
Ag_2CrO_4/g-C_3N_4/GO	Gas phase	300 W Xe lamp and a 420 nm cutoff filter	1.03 μmol g^{-1}	159
Carbon-coated In_2O_3 nanobelts	Aqueous, Pt co-catalyst, and TEOA	300 W Xe lamp	CO, 126.6 μmol h^{-1}; CH_4, 27.9 μmol h^{-1}	149

TABLE III. (*Continued.*)

Materials	Reaction condition	Irradiation	Evolution rate/ yield/TCEN/AQY/AQE	Reference
Pt NPs on TiO_2/SiO_2	0.5 M Na_2SO_4 solution	300 W Xe lamp and simulated solar	CH_4, 9.7 μmol g^{-1} h^{-1}; CO, 1.8 μmol g^{-1} h^{-1}; H_2, 58.7 μmol g^{-1} h^{-1}, reacted electron rate of 198 μmol g^{-1} h^{-1}	163

reported for CO_2 reduction include Ag nano-cube-Re-containing MOF,[97] $CsPbBr_3$,[26] g-C_3N_4/SnS_2,[23] $In_2S_3/CdIn_2S_4$ nanotubes,[64] $TiO_2/CuInS_2$,[85] and zeolitic imidazolate framework-8 nanoclusters on g-C_3N_4 nanotubes.[75] Ti^{3+}—TiO_2,[33] g-C_3N_4/nanocarbon/$ZnIn_2S_4$,[95] α-Fe_2O_3/g-C_3N_4,[89] N-doped carbon/$NiCo_2O_4$ double-shelled nanoboxes,[55] $ZnIn_2S_4$—In_2O_3,[70] Ag_2CrO_4/g-C_3N_4/graphene oxide,[159] Ag dimer/$ZnIn_2S_4$ nanosheets/TiO_2 nanofibers,[60] Au@TiO_2 yolk-shell hollow spheres,[144] carbon-coated In_2O_3[149] g-C_3N_4 co-modified with MnO_x and Au—TiO_2[150] boron-doped g-C_3N_4/anatase titania nanocomposite,[146] and Au/BiOI/MnO_x[162] TiO_2—MnO_x—Pt.[172] Similar to water splitting, 2D carbon-based materials such as graphene-based materials[173] and g-C_3N_4[42,50,173] are very commonly investigated, with g-C_3N_4 attracting increasing attention in recent years. These materials can serve as photocatalyst supports or can be used directly as photocatalysts, and they have been extensively reviewed.[173] Literature reports are summarized in Table III.

Similar to water splitting, for CO_2 reduction, AQE is defined as the number of reacted electrons divided by the number of incident photons and is the parameter of interest.[6] However, CO_2 reduction would typically generate different reaction products. Thus, efficiency is often described using the total consumed electron number (TCEN).[6] However, this number takes into account the reactor volume, catalyst mass, and reaction time,[6] which makes direct comparisons of different materials difficult. Compared to water splitting, AQE/AQY values have been reported considerably less frequently for CO_2 reduction, and they are typically in the range of several percent.[146,150] TCEN is more commonly reported,[6] but in this case as well, huge variation among different literature reports can be observed. Thus, the entire field of photocatalytic fuel generation would benefit from some standardization of experimental conditions, the development of standard test reactor configurations, and requirements for standardized reporting. This would enable direct comparisons between different materials, which would likely facilitate faster development of improved performance photocatalysts. While at present relative comparisons to either P25 or pure g-C_3N_4 can provide some information, this is insufficient for designed development of efficient photocatalysts.

E. Chemical synthesis reactions

Visible-light photocatalysis can also be used in chemical synthesis, for example, to achieve milder reaction conditions, such as lower synthesis temperature, or to replace toxic or expensive reagents depending on the type of chemical reaction.[174] The process has been recently reviewed, from the perspective of chemical reactions that can be achieved[174] or combinations of metallocatalysis and photocatalysis[5] or organocatalysis and photocatalysis.[175] The reactions where the use of photocatalysis was reported include C—C bond formation,[174,176] carbon-heteroatom bond formation, α-amine functionalization, decarboxylative coupling, cycloadditions, atom-transfer radical addition, and fluorination.[174] Some impressive improvements, such as the achievement of the Suzuki–Miyaura coupling reaction at room temperature[176] and progress in the synthesis of trifluoromethoxy and difluoromethoxy compounds, which are of interest in drug development,[177] have been reported. The expanded range of transformations and improvement in the reaction conditions have been achieved for a variety of chemical reactions, with the benefits ranging from marginal to transformative depending on the specific reaction.[174] A variety of photocatalyst materials can be used for this purpose, including those common in other applications, such as TiO_2[178] and carbon nitride.[179]

IV. ADVANCES IN CHARACTERIZATION TECHNIQUES AND UNDERSTANDING OF THE PHYSICAL MECHANISMS

Understanding the mechanisms responsible for a photocatalytic activity of a material for a given reaction and evaluating practical applicability of that material requires comprehensive experimental characterization. The experimental characterization needs to include its optical properties (which for powder nanomaterial samples requires the use of diffuse reflectance UV-Vis spectroscopy), sample morphology [which typically requires scanning electron microscopy (SEM) or transmission electron microscopy (TEM)], sample composition [using energy dispersive x-ray spectroscopy, x-ray photoelectron spectroscopy (XPS), x-ray diffraction, and Raman spectroscopy], and surface properties [using XPS, Raman, and Fourier Transform Infrared spectroscopy (FTIR)].[106] In addition, information about surface area can be obtained from Brunauer–Emmett–Teller (BET) surface area measurements, and relevant particle aggregation size and zeta potential in the medium of interest can be obtained from dynamic light scattering (DLS) measurements.[106] Additional characterization can include determination of energy levels either by cyclic voltammetry or by ultraviolet photoelectron spectroscopy (UPS). In-doped materials for low dopant concentrations, more sensitive composition analysis techniques may be needed, such as atomic absorption spectroscopy (AAS), inductively coupled plasma mass spectroscopy (ICP-MS), or ICP atomic

emission spectroscopy (ICP-AES).[106] Further information on photogenerated charge carrier dynamics can be obtained from photoluminescence and time resolved-photoluminescence measurements. Additional experimental techniques may be employed to evaluate the nature of defects in a semiconductor, such as electron spin resonance (ESR)/electron paramagnetic resonance (EPR) for defects with unpaired electrons.[19]

The evaluation of photocatalytic performance should, in addition to the determination of the experimental rate of the photocatalyzed reaction determined from experiments done on samples where equilibrium in the dark has been achieved, contain the determination of apparent quantum yield or apparent quantum efficiency.[106] It should be noted that the correct determination of these quantities can be complex, but it should be performed to enable reliable comparisons among different research groups.[106] Finally, it is also a good practice to demonstrate data reproducibility by performing the experiment multiple times and including error bars.[106] Stability is also of relevance for practical applications, and it can be evaluated by recovering the photocatalyst and performing repeated cycles on re-used photocatalysts, combined with the characterization of photocatalyst properties after re-use.[106] Furthermore, in the investigations of the reaction mechanisms, the use of isotopes ($^{13}CO_2$ and D_2O)[150] is a highly valuable tool for unambiguous identification of reaction pathways. This is particularly important in CO_2 reduction, where a carbon containing residue (for example, from organic solvents and precursors employed in material synthesis) decomposing under irradiation could be an alternative source of detected reaction products.[6,171] In addition, while oxygen is expected to be generated from CO_2 reduction using water as an electron (hydrogen) source, very few studies report oxygen evolution.[171]

In addition to these necessary characterization techniques, recent development of characterization techniques has provided more insights into the photocatalysis process.[180] In particular, *in situ* or *operando* techniques have facilitated narrowing the pressure gap and enabled a direct observation of the photocatalytic process as well as the surface structural changes in the photocatalysts. Traditional x-ray photoelectron spectroscopy (XPS) is a useful tool to study the elemental surface composition and the oxidation states of the catalysts, but it has to work under ultra-high vacuum environment. Recent advances of the *in situ*/*operando* near ambient pressure XPS (NAP-XPS) technique have allowed probing the underlying mechanism of the catalytic process under a more realistic condition.[181–183] Separating the reaction chamber and the energy analyzer with a specially designed nozzle and a differential pumping system, the NAP-XPS system could collect photoelectrons at a pressure of up to ~20 mbar.[184] Currently, there are two designs for the reaction chamber: backfilling and reaction cell [Figs. 7(a) and 7(b)]. In both cases, there is a nozzle which acts as a slit or an aperture to separate the reaction environment and the high vacuum environment of differential pumping states. The nozzle head is placed close to the sample surface so that it is within the range of the inelastic scattering mean free path (λ) in order to minimize the kinetic energy loss of the photoelectrons. In the differential pumping unit, there are typically three pumping stages with electrostatic lenses installed to change the natural trajectory of the photoelectrons in order to maximize their collection [Fig. 7(c)]. The advantage of the NAP system is that *ex situ* XPS studies of the catalyst before and after the reaction could not access the authentic chemistry of the catalyst surface during the reaction. In particular, inconsistent information could be generated as the used or unused catalysts are measured at room temperature in UHV for *ex situ* studies, while the catalyst at the catalysis state could be at a high temperature in the mixture of reactants. Usefulness of this technique in improving the understanding of fundamental mechanisms responsible for the behavior of specific photocatalysts has been demonstrated. For instance, the technique has revealed the surface chemistry changes of TiO_2 under water vapor and oxygen condition with and without UV irradiation.[185] It has been found that the presence of both water and oxygen is sufficient to sustain the catalytic capability of TiO_2 without photons for a period of time. In addition, the *in situ* irradiated XPS technique can be used to confirm the formation of a direct Z-scheme heterojunction.[87]

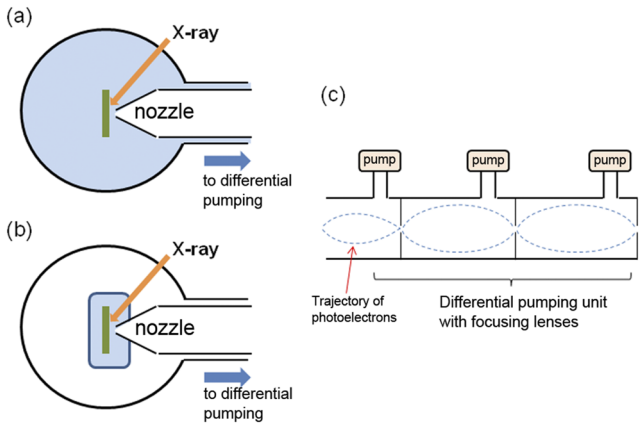

FIG. 7. Schematic diagram of reaction chamber designs in NAP-XPS. (a) Backfilling design. (b) Reaction cell design. (c) Differential pumping system with electrostatic lenses.

Another *in situ* technique is the environmental transmission electron microscopy (E-TEM). Microstructural and chemical changes in the catalysts during an interaction with gas or liquid can be observed by this system up to several mbar with specially designed sample holders.[186] These types of experimental setups are very system-specific with customized design. The sample is normally tilted with respect to the holder tip plane to allow exposure to light and electrons at the same time. The light source for the reaction could be introduced either by lens modules or by fiber optics.[186] The lens-based system has a hollow holder shaft for the optical path (Fig. 8). A laser diode is used to provide illumination, and therefore, the choice of wavelength would be limited by the available laser diodes. As it is connected directly to the microscope vacuum system, the light source cannot be exchanged while the holder is in operation. Once it is evacuated, the heat produced by the laser diode during operation does not dissipate and, hence, the laser efficiency might not be constant over time. The fiber optic design could offer more feasibility for the connection of light sources, but the intensity of illumination will be limited. The two designs in combination have offered complementary options for the *ex situ* experiment. For example, the photo-corrosion of Cu_2O in a water vapor environment under UV illumination was studied by E-TEM with both designs and gave the same result. With *in situ* selected area electron diffraction, a change from Cu_2O to metallic Cu during the reaction could be observed.[186]

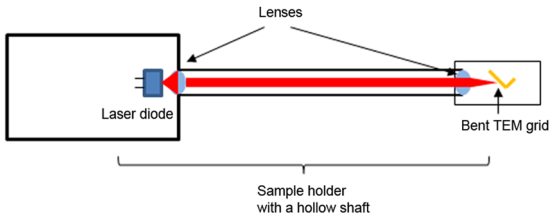

FIG. 8. Schematic diagram of a lens-based system for light introduction into environmental TEM.

Since all the photocatalysis reactions happen on the surface, scanning tunneling microscopy (STM) is an ideal tool to provide information of the adsorption sites, active sites, as well as surface reconstruction of the catalysts. With the development of *in situ* reaction cells, high pressure STM (HP-STM), which allows STM observation under a reacting gas environment up to 100 mbar, has become more mature in the past decade.[187] The core unit of the HP-STM system is the *in situ* reaction cell (Fig. 9). It consists of the sample stage, heating facility, tip and scanning motors, and gas inlet system, and it is isolated from the main chamber. While the cell can be filled with reaction gas up to 100 mbar during *operando* reactions, the base pressure in the main chamber is maintained under UHV condition by using the differential pumping system. Therefore, the changes in morphologies, defects, or vacancies on the surface under reaction conditions can be recorded directly. For instance, metal and metal oxide catalysts were found to have different restructuring processes under different gas content exposure by HP-STM,[187] where this information could not be determined with the *ex situ* experiment. For example, nanoclusters were observed during the exposure of Pt to 1 Torr of O_2 at room temperature and were identified as Pt surface oxide.[187] The clusters on the surface disappeared after evacuating O_2 to UHV. Another example is the reconstruction of the ZnO non-polar surface under different gaseous environments. It was previously found that adsorption of water molecules on the surface can lead to certain reconstruction of the surface. With HP-STP, it was determined that hydrogen is also capable of producing similar reconstruction.[187] To introduce illumination in HP-STM, fiber

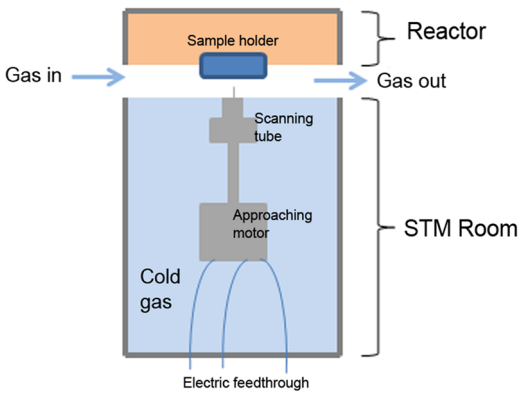

FIG. 9. Schematic diagram of a reaction cell in HP-STM.

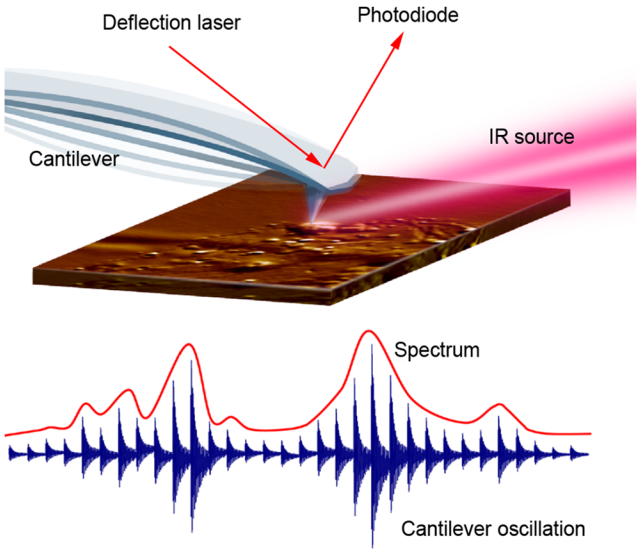

FIG. 10. Schematic diagram of AFM-IR.

optics is a better choice as the lens module may affect the cooling efficiency of the STM.

The atomic force microscope based infrared spectroscopy (AFM-IR) is another recently developed tool to study the spatial chemical change in the surface in nanometer scale, which could be useful for *in situ* reaction investigation.[188] Instead of using the optical method to determine the absorption of infrared light, it makes use of the AFM tip to detect the thermal expansion during the infrared illumination (Fig. 10). The technique has realized up to a 5–10 nm spatial resolution of chemical mapping. It operates in ambient environment, and therefore, the chemical change in the solid surface during a photocatalytic reaction under atmospheric pressure can be determined on site. For instance, a nanoscale degradation study on oil paints that contain titania as inorganic pigments was performed with the AFM-IR instruments.[189] In addition, *in vivo* discrimination of gram-positive and gram-negative bacteria was also feasible with the technique, which could possibly extend to the studies of photocatalytic antibacterial effects.[190]

V. CONCLUSIONS AND FUTURE OUTLOOK

Among photocatalyst materials, the most promising approaches involve the use of complex multicomponent systems, such as heterojunction (including Z-scheme) photocatalysts, combined with co-catalysts and/or plasmonic particles. There is significant interest in the development of non-noble-metal plasmonic particles and co-catalysts to reduce the cost of the photocatalyst. However, what should also be considered is that even with the use of noble metals, efficiency targets have not been reached. In fact, in fuel generation applications, improvements of several orders of magnitude are needed when it comes to efficiency. Therefore, focusing on achieving as high efficiency as possible, combined with comprehensive material characterization and standardization of experimental conditions

and test reactor design, and reporting AQE/AQY values instead of simply reporting reaction rates is expected to contribute to the advance of the field in a more significant manner.

When it comes to practical applications, commercialization potential is often discussed taking into account the estimated cost of generated products or estimated photocatalyst costs,[171] but the challenges of scaling up the production are rarely considered. As already discussed, photocatalysis is impractical for large scale water treatment applications since it is not cost-effective or energy effective when scaled up to industrial level.[15,126] The median E_{EO} value of the reported literature estimates for a photocatalytic process is 335 kW h/m^3/order, which is significantly higher compared to ozonization (0.15 kW h/m^3/order), O_3/H_2O_2 (0.2 kW h/m^3/order), and UV/ozone and UV/hydrogen peroxide (0.7 kW h/m^3/order and 0.75 kW h/m^3/order, 0.15 kW h/m^3/order, respectively).[127] Furthermore, the median E_{EO} values for the UV/H_2O_2 process decrease with increased capacity from lab-scale over pilot-scale to industrial scale.[127] In contrast, the energy consumption of a photocatalytic system increases on scaling up due to pumping and photocatalyst recovery requirements.[126] Consequently, in the only commercial photocatalytic water treatment system, Purifics Photo-cat intended for small-scale applications, the efficiency of the unit improved by replacing the titanium dioxide photocatalyst with hydrogen peroxide.[126] This would become even more pronounced when moving from pilot-scale to industrial scale water treatment due to the need to operate at higher pumping rates. Thus, a possible solution would be to focus on various niche applications,[15] such as small-scale point-of-use systems, or alternatively permanent pollutant degradation regardless of the cost (i.e., photocatalysis can degrade pollutants that are difficult to degrade by other methods), if this ever becomes a social necessity due to increasing pollution levels. Another possible way forward is to focus on optimizing the reactor designs, including the illumination sources such as UV-LEDs.[191,192] UV-LEDs would be particularly suitable for small-scale systems.

In terms of photocatalysis for fuel generation, no reported photocatalyst has come close to the required efficiency level for commercialization, and this is even without considering the technological challenges of scaling up to develop a system to be able to produce fuels at sufficient rates and quantities to be practically usable. It is estimated that the required solar-to-hydrogen efficiency for practical applications is 10% for overall water splitting.[9,166] For reference, current particulate photocatalysts can only achieve ≈1% under laboratory conditions,[166] which means improvement in the efficiency of more than one order of magnitude to obtain 10% efficiency in an industrial scale process. It should be noted that 10% efficiency under solar illumination could not be achieved with photocatalysts with absorption edges at or below 500 nm even for AQY of 100%.[9] In contrast, if the absorption edge could be extended to 600 nm, needed AQY would be 60%.[9] While the majority of review papers tend to discuss issues related to efficiency improvement challenges, it would be worthwhile to consider the challenges of scaling up. For example, a fuel cell of 1 kW consumes approximately 10 l of hydrogen per minute, which means either huge scale up of bench top reactors is required or some efficient method of storage is needed for photocatalytic hydrogen production to be practically relevant. The system lifetime also needs to be evaluated (and it should be noted that more narrow bandgap photocatalysts that are desirable from increasing STH point of view generally have inferior photostability), as well as safety issues, namely, the separation of oxygen and hydrogen when they are produced at large quantities. Estimates of economic realities for methanol generation from CO_2 reduction are similarly pessimistic. It was claimed that solar-to-fuel efficiency as high as 15% needs to be achieved to be economically competitive for methanol generation.[193] This involves huge challenges of 40% one-pass conversion of CO_2 and the achievement of methanol yield rate of ≈10 000 μmol/g_{cat}h.[193] It should be noted that these estimates are based on a number of assumptions made considering the cost estimates of a "solar refinery."[193] Furthermore, one of the reasons for the requirement of high solar-to-fuel efficiency is to reduce the sensitivity to solar irradiance and operational time.[193] Nevertheless, considering typical figures reported so far,[6] the achieved catalytic activity and fuel yields still need to be improved by several orders of magnitude in order to generate meaningful quantities of fuel.

Consequently, there are significant challenges in applications of photocatalysis at industrial scale. On the other hand, niche applications and small-scale systems may be viable and perhaps it would be more meaningful to focus on those. Increased collaboration between physicists, chemists, materials scientists, and engineers is needed to address the challenges of scaling up, and industry input is needed to reduce the gap between academic interest and practical application needs. Considering the efficiency challenges for visible-light photocatalysts to become relevant for practical applications, working on increasing the efficiency is considerably more significant than the development of alternative, lower cost materials. Furthermore, the robustness of the material should not be disregarded since it is highly relevant for the operation of slurry reactors and successful photocatalyst recovery, and some fragile multicomponent materials would simply not survive high pressures, high flow rates, and ultrafiltration recovery in a realistic industrial system.

ACKNOWLEDGMENTS

Financial support from the Seed Funding Grant for Applied and Translational Research, the University of Hong Kong, is acknowledged.

DATA AVAILABILITY

Data sharing is not applicable to this article as no new data were created or analyzed in this study.

REFERENCES

[1] J. X. Low, J. G. Yu, M. Jaroniec, S. Wageh, and A. A. Al-Ghamdi, Adv. Mater. **29**, 1601694 (2017).
[2] F. K. Kessler, Y. Zheng, D. Schwarz, C. Merschjann, W. Schnick, X. C. Wang, and M. J. Bojdys, Nat. Rev. Mater. **2**, 17030 (2017).
[3] C. B. Ong, L. Y. Ng, and A. W. Mohammad, Renewable Sustainable Energy Rev. **81**, 536–551 (2018).
[4] J. W. Fu, J. G. Yu, C. J. Jiang, and B. Cheng, Adv. Energy Mater. **8**, 1701503 (2018).
[5] J. Twilton, C. C. Le, P. Zhang, M. H. Shaw, R. W. Evans, and D. W. C. MacMillan, Nat. Rev. Chem. **1**, 0052 (2017).
[6] K. Li, B. Peng, and T. Y. Peng, ACS Catal. **6**, 7485–7527 (2016).
[7] Q. J. Xiang, B. Cheng, and J. G. Yu, Angew. Chem., Int. Ed. **54**, 11350–11366 (2015).

[8]A. Dhakshinamoorthy, A. M. Asiri, and H. Garcia, Angew. Chem., Int. Ed. **55**, 5414–5445 (2016).
[9]S. S. Chen, T. Takata, and K. Domen, Nat. Rev. Mater. **2**, 17050 (2017).
[10]K. Honda and A. Fujishima, Nature **238**, 37 (1972).
[11]H. Reiche and A. J. Bard, J. Am. Chem. Soc. **101**, 3127–3128 (1979).
[12]N. Farhadian, R. Akbarzadeh, M. Pirsaheb, T. C. Jen, Y. Fakhri, and A. Asadi, Int. J. Biol. Macromol. **132**, 360–373 (2019).
[13]S. Li and J. Y. Hu, Water Res. **132**, 320–330 (2018).
[14]K. Wetchakun, N. Wetchakun, and S. Sakulsermsuk, J. Ind. Eng. Chem. **71**, 19–49 (2019).
[15]S. K. Loeb, P. J. J. Alvarez, J. A. Brame, E. L. Cates, W. Y. Choi, J. Crittenden, D. D. Dionysiou, Q. Li, G. Li-Puma, X. Quan, D. L. Sedlak, T. D. Waite, P. Westerhoff, and J.-H. Kim, Environ. Sci. Technol. **53**, 2937–2947 (2019).
[16]M. Ge, C. Cao, J. Huang, S. Li, Z. Chen, K.-Q. Zhang, S. S. Al-Deyab, and Y. Lai, J. Mater. Chem. A **4**, 6772–6801 (2016).
[17]L. B. Jiang, X. Z. Yuan, G. M. Zeng, J. Liang, Z. B. Wu, and H. Wang, Environ. Sci.: Nano **5**, 599–615 (2018).
[18]H. Wang, W. D. Zhang, X. W. Li, J. Y. Li, W. L. Cen, Q. Y. Li, and F. Dong, Appl. Catal., B **225**, 218–227 (2018).
[19]H. Li, J. Li, Z. H. Ai, F. L. Jia, and L. Z. Zhang, Angew. Chem., Int. Ed. **57**, 122–138 (2018).
[20]Y. Zheng, Z. H. Yu, H. H. Ou, A. M. Asiri, Y. L. Chen, and X. C. Wang, Adv. Funct. Mater. **28**, 1705407 (2018).
[21]X. J. Zhu, T. M. Zhang, Z. J. Sun, H. L. Chen, J. Guan, X. Chen, H. X. Ji, P. W. Du, and S. F. Yang, Adv. Mater. **29**, 1605776 (2017).
[22]A. Behera, D. Kandi, S. M. Majhi, S. Martha, and K. Parida, Beilstein J. Nanotechnol. **9**, 436–446 (2018).
[23]T. M. Di, B. C. Zhu, B. Cheng, J. G. Yu, and J. S. Xu, J. Catal. **352**, 532–541 (2017).
[24]Y. Wang, S. Z. F. Phua, G. Dong, X. Liu, B. He, Q. Zhai, Y. Li, C. Zheng, H. Quan, Z. Li, and Y. Zhao, Chem **5**, 2775–2813 (2019).
[25]J. D. Xiao, Q. Z. Han, Y. B. Xie, J. Yang, Q. Z. Su, Y. Chen, and H. B. Cao, Environ. Sci. Technol. **51**, 13380–13387 (2017).
[26]Y. F. Xu, M. Z. Yang, B. X. Chen, X. D. Wang, H. Y. Chen, D. B. Kuang, and C. Y. Su, J. Am. Chem. Soc. **139**, 5660–5663 (2017).
[27]V. S. Vyas, V. W.-H. Lau, and B. V. Lotsch, Chem. Mater. **28**, 5191–5204 (2016).
[28]S. Xie, Q. Zhang, G. Liu, and Y. Wang, Chem. Commun. **52**, 35–59 (2016).
[29]S. G. Kumar and K. S. R. K. Rao, Appl. Surf. Sci. **391**, 124–148 (2017).
[30]X. Liu, G. Du, and M. Li, ACS Omega **4**, 14902–14912 (2019).
[31]R. Hailili, X. Yuan, and C. Wang, Catal. Today **335**, 591–598 (2019).
[32]J. Di, C. Chen, C. Zhu, P. Song, J. Xiong, M. Ji, J. Zhou, Q. Fu, M. Xu, W. Hao, J. Xia, S. Li, H. Li, and Z. Liu, ACS Appl. Mater. Interfaces **11**, 30786–30792 (2019).
[33]K. Sasan, F. Zuo, Y. Wang, and P. Y. Feng, Nanoscale **7**, 13369–13372 (2015).
[34]H. Wang, D. Y. Yong, S. C. Chen, S. L. Jiang, X. D. Zhang, W. Shao, Q. Zhang, W. S. Yan, B. C. Pan, and Y. Xie, J. Am. Chem. Soc. **140**, 1760–1766 (2018).
[35]H. J. Yu, R. Shi, Y. X. Zhao, T. Bian, Y. F. Zhao, C. Zhou, G. I. N. Waterhouse, L. Z. Wu, C. H. Tung, and T. R. Zhang, Adv. Mater. **29**, 1605148 (2017).
[36]J. Huang, Y. Cao, H. Wang, H. Yu, F. Peng, H. Zou, and Z. Liu, Chem. Eng. J. **373**, 687–699 (2019).
[37]C. Yang, Z. Xue, J. Qin, M. Sawangphruk, X. Zhang, and R. Liu, Appl. Catal., B **259**, 118094 (2019).
[38]N. Zhang, C. Gao, and Y. Xiong, J. Energy Chem. **37**, 43–57 (2019).
[39]L. Lin, J. Huang, X. Li, M. A. Abass, and S. Zhang, Appl. Catal., B **203**, 615–624 (2017).
[40]H. W. Huang, K. Xiao, N. Tian, F. Dong, T. R. Zhang, X. Du, and Y. H. Zhang, J. Mater. Chem. A **5**, 17452–17463 (2017).
[41]Z. W. Tong, D. Yang, Z. Li, Y. H. Nan, F. Ding, Y. C. Shen, and Z. Y. Jiang, ACS Nano **11**, 1103–1112 (2017).
[42]P. F. Xia, B. C. Zhu, J. G. Yu, S. W. Cao, and M. Jaroniec, J. Mater. Chem. A **5**, 3230–3238 (2017).
[43]J. Liu, Z. Wei, and W. Shangguan, Chemcatchem **11**, 6177 (2019).
[44]L. Ruan, X. Wang, T. Wang, Z. Ren, Y. Chen, R. Zhao, D. Zhou, G. Fu, S. Li, L. Gao, Y. Lu, Z. Wang, H. Tian, X. Kong, and G. Han, ACS Appl. Mater. Interfaces **11**, 37256–37262 (2019).
[45]J. L. Ge, Y. F. Zhang, Y. J. Heo, and S. J. Park, Catalysts **9**, 122 (2019).
[46]L. Wang, D. Wu, Z. Guo, J. Yan, Y. Hu, Z. Chang, Q. Yuan, H. Ming, and J. Wang, J. Alloys Compd. **745**, 26–32 (2018).
[47]M. Pylnev and M.-S. Wong, J. Photochem. Photobiol., A **378**, 125–130 (2019).
[48]W. Zhang, Y. Li, X. Fan, F. Zhang, G. Zhang, Y.-A. Zhu, W. Peng, S. Wang, and X. Duan, Carbon **155**, 268–278 (2019).
[49]N. Tian, Y. H. Zhang, X. W. Li, K. Xiao, X. Du, F. Dong, G. I. N. Waterhouse, T. R. Zhang, and H. W. Huang, Nano Energy **38**, 72–81 (2017).
[50]J. W. Fu, B. C. Zhu, C. J. Jiang, B. Cheng, W. You, and J. G. Yu, Small **13**, 1603938 (2017).
[51]J. Jiang, S. W. Cao, C. L. Hu, and C. H. Chen, Chin. J. Catal. **38**, 1981–1989 (2017).
[52]C. Y. Liu, Y. H. Zhang, F. Dong, A. H. Reshak, L. Q. Ye, N. Pinna, C. Zeng, T. R. Zhang, and H. W. Huang, Appl. Catal., B **203**, 465–474 (2017).
[53]S. S. Menon, H. Y. Hafeez, B. Gupta, K. Baskar, G. Bhalerao, S. Hussain, B. Neppolian, and S. Singh, Renewable Energy **141**, 760–769 (2019).
[54]Z. Li, F. Zhang, J. Han, J. Zhu, M. Li, B. Zhang, W. Fan, J. Lu, and C. Li, Catal. Lett. **148**, 933–939 (2018).
[55]S. B. Wang, B. Y. Guan, and X. W. D. Lou, Energy Environ. Sci. **11**, 306–310 (2018).
[56]A. Behera, D. Kandi, S. Martha, and K. Parida, Inorg. Chem. **58**, 16592–16608 (2019).
[57]M. T. Uddin, Y. Nicolas, C. Olivier, W. Jaegermann, N. Rockstroh, H. Junge, and T. Toupance, Phys. Chem. Chem. Phys. **19**, 19279–19288 (2017).
[58]M. H. Huang and M. Madasu, Nano Today **28**, 100768 (2019).
[59]Y. Bai, Y. Zhou, J. Zhang, X. Chen, Y. Zhang, J. Liu, J. Wang, F. Wang, C. Chen, C. Li, R. Li, and C. Li, ACS Catal. **9**, 3242–3252 (2019).
[60]Z. Y. Zhang, Y. Z. Huang, K. C. Liu, L. J. Guo, Q. Yuan, and B. Dong, Adv. Mater. **27**, 5906–5914 (2015).
[61]M. Li, F. Y. Liu, Z. Y. Ma, W. Liu, J. L. Liang, and M. P. Tong, Chem. Eng. J. **371**, 750–758 (2019).
[62]J. J. Wang, L. Tang, G. M. Zeng, Y. C. Deng, Y. N. Liu, L. L. Wang, Y. Y. Zhou, Z. Guo, J. J. Wang, and C. Zhang, Appl. Catal., B **209**, 285–294 (2017).
[63]Y. N. Chen, G. Q. Zhu, M. Hojamberdiev, J. Z. Gao, R. L. Zhu, C. H. Wang, X. M. Wei, and P. Liu, J. Hazard. Mater. **344**, 42–54 (2018).
[64]S. B. Wang, B. Y. Guan, Y. Lu, and X. W. D. Lou, J. Am. Chem. Soc. **139**, 17305–17308 (2017).
[65]B. Han, S. Q. Liu, N. Zhang, Y. J. Xu, and Z. R. Tang, Appl. Catal., B **202**, 298–304 (2017).
[66]J. N. Liu, Q. H. Jia, J. L. Long, X. X. Wang, Z. W. Gao, and Q. Gu, Appl. Catal., B **222**, 35–43 (2018).
[67]X. Q. Hao, J. Zhou, Z. W. Cui, Y. C. Wang, Y. Wang, and Z. G. Zou, Appl. Catal., B **229**, 41–51 (2018).
[68]B. Lin, H. Li, H. An, W. B. Hao, J. J. Wei, Y. Z. Dai, C. S. Ma, and G. D. Yang, Appl. Catal., B **220**, 542–552 (2018).
[69]J. R. Ran, W. W. Guo, H. L. Wang, B. C. Zhu, J. G. Yu, and S. Z. Qiao, Adv. Mater. **30**, 1800128 (2018).
[70]S. B. Wang, B. Y. Guan, and X. W. D. Lou, J. Am. Chem. Soc. **140**, 5037–5040 (2018).
[71]F. Zhang, Y. C. Zhang, G. S. Zhang, Z. J. Yang, D. D. Dionysiou, and A. P. Zhu, Appl. Catal., B **236**, 53–63 (2018).
[72]S. Bellamkonda, N. Thangavel, H. Y. Hafeez, B. Neppolian, and G. R. Rao, Catal. Today **321**, 120–127 (2019).
[73]K. K. Das, S. Patnaik, S. Mansingh, A. Behera, A. Mohanty, C. Acharya, and K. Parida, J. Colloid Interface Sci. **561**, 551–567 (2020).
[74]S. Patnaik, K. K. Das, A. Mohanty, and K. Parida, Catal. Today **315**, 52–66 (2018).
[75]S. W. Liu, F. Chen, S. T. Li, X. X. Peng, and Y. Xiong, Appl. Catal., B **211**, 1–10 (2017).
[76]Y. F. Zhang and S. J. Park, Appl. Catal., B **240**, 92–101 (2019).

[77]A. Chauhan, M. Rastogi, P. Scheier, C. Bowen, R. V. Kumar, and R. Vaish, Appl. Phys. Rev. **5**, 041111 (2018).
[78]D. L. Huang, S. Chen, G. M. Zeng, X. M. Gong, C. Y. Zhou, M. Cheng, W. J. Xue, X. L. Yan, and J. Li, Coord. Chem. Rev. **385**, 44–80 (2019).
[79]Y. O. Wang, H. Suzuki, J. J. Xie, O. Tomita, D. J. Martin, M. Higashi, D. Kong, R. Abe, and J. Tang, Chem. Rev. **118**, 5201–5241 (2018).
[80]Z. Mo, H. Xu, Z. G. Chen, X. J. She, Y. H. Song, J. B. Lian, X. W. Zhu, P. C. Yan, Y. C. Lei, S. Q. Yuan, and H. M. Li, Appl. Catal., B **241**, 452–460 (2019).
[81]Q. Xu, L. Zhang, J. Yu, S. Wageh, A. A. Al-Ghamdi, and M. Jaroniec, Mater. Today **21**, 1042–1063 (2018).
[82]F. Chen, Q. Yang, X. M. Li, G. M. Zeng, D. B. Wang, C. G. Niu, J. W. Zhao, H. X. An, T. Xie, and Y. C. Deng, Appl. Catal., B **200**, 330–342 (2017).
[83]S. Adhikari, S. Mandal, and D.-H. Kim, Chem. Eng. J. **373**, 31–43 (2019).
[84]T. T. Xiao, Z. Tang, Y. Yang, L. Q. Tang, Y. Zhou, and Z. G. Zou, Appl. Catal., B **220**, 417–428 (2018).
[85]F. Y. Xu, J. J. Zhang, B. C. Zhu, J. G. Yu, and J. S. Xu, Appl. Catal., B **230**, 194–202 (2018).
[86]A. Y. Meng, B. C. Zhu, B. Zhong, L. Y. Zhang, and B. Cheng, Appl. Surf. Sci. **422**, 518–527 (2017).
[87]J. X. Low, B. Z. Dai, T. Tong, C. J. Jiang, and J. G. Yu, Adv. Mater. **31**, 1802981 (2019).
[88]X. J. She, J. J. Wu, H. Xu, J. Zhong, Y. Wang, Y. H. Song, K. Q. Nie, Y. Liu, Y. C. Yang, M.-T. F. Rodrigues, R. Vajtai, J. Lou, D. L. Du, H. M. Li, and P. M. Ajayan, Adv. Energy Mater. **7**, 1700025 (2017).
[89]Z. F. Jiang, W. M. Wan, H. M. Li, S. Q. Yuan, H. J. Zhao, and P. K. Wong, Adv. Mater. **30**, 1706108 (2018).
[90]W. L. Yu, J. X. Chen, T. T. Shang, L. F. Chen, L. Gu, and T. Y. Peng, Appl. Catal., B **219**, 693–704 (2017).
[91]Q. Wang, T. Hisatomi, Y. Suzuk, Z. H. Pan, J. Seo, M. Katayama, T. Minegishi, H. Nishiyama, T. Takata, K. Seki, A. Kudo, T. Yamada, and K. Domen, J. Am. Chem. Soc. **139**, 1675–1683 (2017).
[92]W. K. Jo and N. C. S. Selvam, Chem. Eng. J. **317**, 913–924 (2017).
[93]M. S. Zhu, Z. C. Sun, M. Fujitsuka, and T. Majima, Angew. Chem., Int. Ed. **57**, 2160–2164 (2018).
[94]D. Z. Lu, H. M. Wang, X. N. Zhao, K. K. Kondamareddy, J. Q. Ding, C. H. Li, and P. F. Fang, ACS Sustainable Chem. Eng. **5**, 1436–1445 (2017).
[95]F. F. Shi, L. L. Chen, M. Chen, and D. L. Jiang, Chem. Commun. **51**, 17144–17147 (2015).
[96]Q. Jiang, C. Ji, D. J. Riley, and F. Xie, Nanomaterials **9**, 1 (2019).
[97]K. M. Choi, D. Kim, B. Rungtaweevoranit, C. A. Trickett, J. T. D. Barmanbek, A. S. Alshammari, P. D. Yang, and O. M. Yaghi, J. Am. Chem. Soc. **139**, 356–362 (2017).
[98]K. K. Paul, P. K. Giri, H. Sugimoto, M. Fujii, and B. Choudhury, Sol. Energy Mater. Sol. Cells **201**, 110053 (2019).
[99]S. K. Ray, D. Dhakal, G. Gyawali, B. Joshi, A. R. Koirala, and S. W. Lee, Chem. Eng. J. **373**, 259–274 (2019).
[100]J. J. Wang, L. Tang, G. M. Zeng, Y. N. Liu, Y. Y. Zhou, Y. C. Deng, J. J. Wang, and B. Peng, ACS Sustainable Chem. Eng. **5**, 1062–1072 (2017).
[101]J. Nie, A. O. T. Patrocinio, S. Hamid, F. Sieland, J. Sann, S. Xia, D. W. Bahnemann, and J. Schneider, Phys. Chem. Chem. Phys. **20**, 5264–5273 (2018).
[102]L. M. Guo, Z. Z. Yang, K. Marcus, Z. Li, B. C. Luo, L. Zhou, X. H. Wang, Y. G. Du, and Y. Yang, Energy Environ. Sci. **11**, 106–114 (2018).
[103]Z. Hu, Y. Mi, Y. Ji, R. Wang, W. Zhou, X. Qiu, X. Liu, Z. Fang, and X. Wu, Nanoscale **11**, 16445–16454 (2019).
[104]L. Ma, D.-J. Yang, X.-P. Song, H.-X. Li, S.-J. Ding, L. Xiong, P.-L. Qin, and X.-B. Chen, Sol. RRL **4**, 1900376 (2019).
[105]G. Yu, J. Qian, P. Zhang, B. Zhang, W. Zhang, W. Yan, and G. Liu, Nat. Commun. **10**, 4912 (2019).
[106]M. A. Hoque and M. I. Guzman, Materials **11**, 1990 (2018).
[107]Z. Y. Wu, G. H. Zhao, Y. J. Zhang, J. Liu, Y.-N. Zhang, and H. J. Shi, J. Mater. Chem. A **3**, 3416–3424 (2015).
[108]J. Bai, R. Wang, Y. P. Li, Y. Y. Tang, Q. Y. Zeng, L. G. Xia, X. J. Li, J. H. Li, C. L. Li, and B. X. Zhou, J. Hazard. Mater. **311**, 51–62 (2016).
[109]A. Behera, D. Kandi, S. Sahoo, and K. Parida, J. Phys. Chem. C **123**, 17112–17126 (2019).
[110]W. L. Wang, Q. Y. Wu, N. Huang, Z. B. Xu, M. Y. Lee, and H. Y. Hu, Water Res. **141**, 109–125 (2018).
[111]C. Y. Zhou, C. Lai, D. L. Huang, G. M. Zeng, C. Zhang, M. Cheng, L. Hu, J. Wan, W. P. Xiong, M. Wen, X. F. Wen, and L. Qin, Appl. Catal., B **220**, 202–210 (2018).
[112]C. Y. Zhou, C. Lai, P. Xu, G. M. Zeng, D. L. Huang, C. Zhang, M. Cheng, L. Hu, J. Wan, Y. Liu, W. P. Xiong, Y. C. Deng, and M. Wen, ACS Sustainable Chem. Eng. **6**, 4174–4184 (2018).
[113]Q. Q. Cai and J. Y. Hu, Water Res. **140**, 251–260 (2018).
[114]D. L. Jiang, T. Y. Wang, Q. Xu, D. Li, S. C. Meng, and M. Chen, Appl. Catal., B **201**, 617–628 (2017).
[115]G. S. Zhang, Y. N. Xue, Q. Wang, P. Wang, H. Yao, W. Zhang, J. B. Zhao, and Y. Li, Chemosphere **230**, 406–415 (2019).
[116]H. Wang, Y. Wu, M. B. Feng, W. G. Tu, T. Xiao, T. Xiong, H. X. Ang, X. Z. Yuan, and J. W. Chew, Water Res. **144**, 215–225 (2018).
[117]A. Kumar, A. Kumar, G. Sharma, A. H. Al-Muhtaseb, M. Naushad, A. A. Ghfar, and F. J. Stadler, Chem. Eng. J. **334**, 462–478 (2018).
[118]A. Behera, S. Mansingh, K. K. Das, and K. Parida, J. Colloid Interface Sci. **544**, 96–111 (2019).
[119]A. Behera, D. Kandi, S. Mansingh, S. Martha, and K. Parida, J. Colloid Interface Sci. **556**, 667–679 (2019).
[120]F. L. Wang, Y. F. Wang, Y. P. Feng, Y. Q. Zeng, Z. J. Xie, Q. X. Zhang, Y. H. Su, P. Chen, Y. Liu, K. Yao, W. Y. Lv, and G. G. Liu, Appl. Catal., B **221**, 510–520 (2018).
[121]A. Surenjan, T. Pradeep, and L. Philip, Chemosphere **228**, 629–639 (2019).
[122]N. S. Hassan, A. A. Jalil, N. F. Khusnun, M. W. Ali, and S. Haron, J. Alloys Compd. **789**, 221–230 (2019).
[123]D. N. Zhang, C. G. Lee, H. Javed, P. F. Yu, J. H. Kim, and P. J. J. Alvarez, Environ. Sci. Technol. **52**, 12402–12411 (2018).
[124]M. Camila Ariza-Tarazona, J. Francisco Villarreal-Chiu, V. Barbieri, C. Siligardi, and E. Iveth Cedillo-Gonzalez, Ceram. Int. **45**, 9618–9624 (2019).
[125]T. S. Tofa, K. L. Kunjali, S. Paul, and J. Dutta, Environ. Chem. Lett. **17**, 1341–1346 (2019).
[126]E. L. Cates, Environ. Sci. Technol. **51**, 757–758 (2017).
[127]D. B. Miklos, C. Remy, M. Jekel, K. G. Linden, J. E. Drewes, and U. Huebner, Water Res. **139**, 118–131 (2018).
[128]Y. Choi, M. S. Koo, A. D. Bokare, D.-H. Kim, D. W. Bahnemann, and W. Choi, Environ. Sci. Technol. **51**, 3973–3981 (2017).
[129]K. K. Das, S. Patnaik, B. Nanda, A. C. Pradhan, and K. Parida, ChemistrySelect **4**, 1806–1819 (2019).
[130]Z. J. Li, Z. W. Huang, W. L. Guo, L. Wang, L. R. Zheng, Z. F. Cha, and W. Q. Shi, Environ. Sci. Technol. **51**, 5666–5674 (2017).
[131]J. H. You, Y. Z. Guo, R. Guo, and X. W. Liu, Chem. Eng. J. **373**, 624–641 (2019).
[132]C. Zhang, M. Y. Zhang, Y. Li, and D. M. Shuai, Appl. Catal., B **248**, 11–21 (2019).
[133]P. Ganguly, C. Byrne, A. Breen, and S. C. Pillai, Appl. Catal., B **225**, 51–75 (2018).
[134]N. Pichel, M. Vivar, and M. Fuentes, Chemosphere **218**, 1014–1030 (2019).
[135]C. H. Chu, E. C. Ryberg, S. K. Loeb, M.-J. Suh, and J.-H. Kim, Acc. Chem. Res. **52**, 1187–1195 (2019).
[136]K. L. Nelson, A. B. Boehm, R. J. Davies-Colley, M. C. Dodd, T. Kohn, K. G. Linden, Y. Y. Liu, P. A. Maraccini, K. McNeill, W. A. Mitch, T. H. Nguyen, K. M. Parker, R. A. Rodriguez, L. M. Sassoubre, A. I. Silverman, K. R. Wigginton, and R. G. Zepp, Environ. Sci.: Processes Impacts **20**, 1089–1122 (2018).
[137]J. L. Liang, F. Y. Liu, M. Li, W. Liu, and M. P. Tong, Water Res. **137**, 120–129 (2018).
[138]Y. Boyjoo, H. Q. Sun, J. Liu, V. K. Pareek, and S. B. Wang, Chem. Eng. J. **310**, 537–559 (2017).
[139]Y. Huang, Y. L. Liang, Y. F. Rao, D. D. Zhu, J. j. Cao, Z. X. Shen, W. K. Ho, and S. C. Lee, Environ. Sci. Technol. **51**, 2924–2933 (2017).

[140]Y. F. Jia, S. P. Li, J. Z. Gao, G. Q. Zhu, F. C. Zhang, X. J. Shi, Y. Huang, and C. L. Liu, Appl. Catal., B **240**, 241–252 (2019).
[141]M. Y. Zhu, Q. Liu, W. Chen, Y. Y. Yin, L. Ge, H. Li, and K. Wang, ACS Appl. Mater. Interfaces **9**, 38832–38841 (2017).
[142]S. Shenawi-Khalil, V. Uvarov, S. Fronton, I. Popov, and Y. Sasson, J. Phys. Chem. C **116**, 11004–11012 (2012).
[143]S. C. Yan, Z. S. Li, and Z. G. Zou, Langmuir **25**, 10397–10401 (2009).
[144]W. G. Tu, Y. Zhou, H. J. Li, P. Li, and Z. G. Zou, Nanoscale **7**, 14232–14236 (2015).
[145]K. Maeda and T. E. Mallouk, Bull. Chem. Soc. Jpn. **92**, 38–54 (2019).
[146]F. Raziq, Y. Qu, X. L. Zhang, M. Humayun, J. Wu, A. Zada, H. T. Yu, X. J. Sun, and L. Q. Jing, J. Phys. Chem. C **120**, 98–107 (2016).
[147]H. H. Ou, L. H. Lin, Y. Zheng, P. J. Yang, Y. X. Fang, and X. C. Wang, Adv. Mater. **29**, 1700008 (2017).
[148]Y. G. Tan, Z. Shu, J. Zhou, T. T. Li, W. B. Wang, and Z. L. Zhao, Appl. Catal., B **230**, 260–268 (2018).
[149]Y. X. Pan, Y. You, S. Xin, Y. T. Li, G. T. Fu, Z. M. Cui, Y. L. Men, F. F. Cao, S. H. Yu, and J. B. Goodenough, J. Am. Chem. Soc. **139**, 4123–4129 (2017).
[150]F. Raziq, L. Q. Sun, Y. Y. Wang, X. L. Zhang, M. Humayun, S. Ali, L. L. Bai, Y. Qu, H. T. Yu, and L. Q. Jing, Adv. Energy Mater. **8**, 1701580 (2018).
[151]B. C. Hodges, E. L. Cates, and J.-H. Kim, Nat. Nanotechnol. **13**, 642–650 (2018).
[152]S. Qiu, Y. Shen, G. Wei, S. Yao, W. Xi, M. Shu, R. Si, M. Zhang, J. Zhu, and C. An, Appl. Catal., B **259**, 118036 (2019).
[153]B. Wang, H. Cai, and S. Shen, Small Methods **3**, 1800447 (2019).
[154]L. Zeng, C. Dai, B. Liu, and C. Xue, J. Mater. Chem. A **7**, 24217–24221 (2019).
[155]W. Zhang, Q. Peng, L. Shi, Q. Yao, X. Wang, A. Yu, Z. Chen, and Y. Fu, Small **15**, 1905166 (2019).
[156]L. Wang, W. Chen, D. Zhang, Y. Du, R. Amal, S. Qiao, J. Wu, and Z. Yin, Chem. Soc. Rev. **48**, 5310–5349 (2019).
[157]R. C. Shen, J. Xie, H. D. Zhang, A. P. Zhang, X. B. Chen, and X. Li, ACS Sustainable Chem. Eng. **6**, 816–826 (2018).
[158]J. R. Ran, G. P. Gao, F. T. Li, T. Y. Ma, A. J. Du, and S. Z. Qiao, Nat. Commun. **8**, 13907 (2017).
[159]D. F. Xu, B. Cheng, W. K. Wang, C. J. Jiang, and J. G. Yu, Appl. Catal., B **231**, 368–380 (2018).
[160]R. B. Wei, Z. L. Huang, G. H. Gu, Z. Wang, L. X. Zeng, Y. B. Chen, and Z. Q. Liu, Appl. Catal., B **231**, 101–107 (2018).
[161]Z. M. Pan, Y. Zheng, F. S. Guo, P. P. Niu, and X. C. Wang, ChemSusChem **10**, 87–90 (2017).
[162]Y. Bai, L. Q. Ye, L. Wang, X. Shi, P. Q. Wang, and W. Bai, Environ. Sci.: Nano **3**, 902–909 (2016).
[163]C. Y. Dong, C. Lian, S. C. Hu, Z. S. Deng, J. Q. Gong, M. D. Li, H. L. Liu, M. Y. Xing, and J. L. Zhang, Nat. Commun. **9**, 1252 (2018).
[164]S. W. Cao, Y. Li, B. C. Zhu, M. Jaroniec, and J. G. Yu, J. Catal. **349**, 208–217 (2017).
[165]P. V. Kamat and S. Jin, ACS Energy Lett. **3**, 622–623 (2018).
[166]Z. Wang, C. Li, and K. Domen, Chem. Soc. Rev. **48**, 2109–2125 (2019).
[167]M. S. Zhu, S. Kim, L. Mao, M. Fujitsuka, J. Y. Zhang, X. C. Wang, and T. Majima, J. Am. Chem. Soc. **139**, 13234–13242 (2017).
[168]A. Naseri, M. Samadi, A. Pourjavadi, A. Z. Moshfegh, and S. Ramakrishna, J. Mater. Chem. A **5**, 23406–23433 (2017).
[169]G. G. Zhang, G. S. Li, Z. A. Lan, L. H. Lin, A. Savateev, T. Heil, S. Zafeiratos, X. C. Wang, and M. Antonietti, Angew. Chem., Int. Ed. **56**, 13445–13449 (2017).
[170]Y. J. Yuan, P. Wang, Z. Li, Y. Wu, W. Bai, Y. Su, J. Guan, S. Wu, J. Zhong, Z. T. Yu, and Z. Zou, Appl. Catal., B **242**, 1–8 (2019).
[171]D. N. Chen, X. G. Zhang, and A. F. Lee, J. Mater. Chem. A **3**, 14487–14516 (2015).
[172]A. Y. Meng, L. Y. Zhang, B. Cheng, and J. G. Yu, ACS Appl. Mater. Interfaces **11**, 5581–5589 (2019).
[173]J. X. Low, B. Cheng, J. G. Yu, and M. Jaroniec, Energy Storage Mater. **3**, 24–35 (2016).
[174]L. Marzo, S. K. Pagire, O. Reiser, and B. Koenig, Angew. Chem., Int. Ed. **57**, 10034–10072 (2018).
[175]Y.-Y. Liu, J. Liu, L.-Q. Lu, and W.-J. Xiao, Top. Curr. Chem. **377**, 37 (2019).
[176]Z. Jiao, Z. Zhai, X. Guo, and X.-Y. Guo, J. Phys. Chem. C **119**, 3238–3243 (2015).
[177]J. W. Lee, K. N. Lee, and M.-Y. Ngai, Angew. Chem., Int. Ed. **58**, 11171–11181 (2019).
[178]H. Cheng and W. Xu, Org. Biomol. Chem. **17**, 9977–9989 (2019).
[179]A. Savateev, I. Ghosh, B. Koenig, and M. Antonietti, Angew. Chem., Int. Ed. **57**, 15936–15947 (2018).
[180]C. Z. Luo, X. H. Ren, Z. G. Dai, Y. P. Zhang, X. Qi, and C. X. Pan, ACS Appl. Mater. Interfaces **9**, 23265–23286 (2017).
[181]L. Nguyen, F. F. Tao, Y. Tang, J. Dou, and X.-J. Bao, Chem. Rev. **119**, 6822–6905 (2019).
[182]X. Q. Zhang and S. Ptasinska, Top. Catal. **59**, 564–573 (2016).
[183]A. Kolmakov, L. Gregoratti, M. Kiskinova, and S. Günther, Top. Catal. **59**, 448–468 (2016).
[184]F. F. Tao, ChemCatChem **4**, 583–590 (2012).
[185]P. Krishnan, M. Liu, P. A. Itty, Z. Liu, V. Rheinheimer, M. H. Zhang, P. J. Monteiro, and L. E. Yu, Sci. Rep. **7**, 43298 (2017).
[186]F. Cavalca, A. B. Laursen, B. E. Kardynal, R. E. Dunin-Borkowski, S. Dahl, J. B. Wagner, and T. W. Hansen, Nanotechnology **23**, 075705 (2012).
[187]H. Zhang, H. Sun, K. Shen, J. Hu, J. Hu, Z. Jiang, and F. Song, Materials **12**, 3674 (2019).
[188]A. Dazzi and C. B. Prater, Chem. Rev. **117**, 5146–5173 (2017).
[189]S. Morsch, B. A. van Driel, K. J. van den Berg, and J. Dik, ACS Appl. Mater. Interfaces **9**, 10169–10179 (2017).
[190]K. Kochan, D. Perez-Guaita, J. Pissang, J.-H. Jiang, A. Y. Peleg, D. McNaughton, P. Heraud, and B. R. Wood, J. R. Soc., Interface **15**, 20180115 (2018).
[191]L. Ling, H. Tugaoen, J. Brame, S. Sinha, C. Li, J. Schoepf, K. Hristovski, J.-H. Kim, C. Shang, and P. Westerhoff, Environ. Sci. Technol. **51**, 13319–13326 (2017).
[192]G. Matafonova and V. Batoev, Water Res. **132**, 177–189 (2018).
[193]J. A. Herron and C. T. Maravelias, Energy Technol. **4**, 1369–1391 (2016).
[194]L. Q. Tang, R. Chen, X. G. Meng, B. H. Lv, F. T. Fan, J. H. Ye, X. Y. Wang, Y. Zhou, C. Li, and Z. G. Zou, Chem. Commun. **54**, 5126–5129 (2018).
[195]Z. Y. Zhao and W. W. Dai, Inorg. Chem. **53**, 13001–13011 (2014).
[196]Y. Xu and M. A. Schoonen, Am. Mineral. **85**, 543–556 (2000).